의학박사 학위논문

Discovery and verification of blood-based protein biomarker candidates for prediction of acute graft-versus-host disease and non-relapse mortality by using mass spectrometry-based proteomics approaches

질량분석기 기반의 단백질체학 방법론을 이용하여 이식편대숙주병의 발병위험 및 무재발사망률 예측을 위한 혈액 단백질 생체표지자의 발굴 및 검증 연구

2018년 8월

서울대학교 대학원

임상의과학과

단 기 순

A thesis of the Degree of Doctor of Philosophy

질량분석기 기반의 단백질체학 방법론을 이용하여 이식편대숙주병의 발병위험 및 무재발 사망률 예측을 위한 혈액 단백질 생체표지자의 발굴 및 검증 연구

Discovery and verification of blood-based protein biomarker candidates for prediction of acute graft-versus-host disease and non-relapse mortality by using mass spectrometry-based proteomics approaches

August 2018

Major in Clinical Medical Sciences
Department of Clinical Medical Sciences
College of Medicine, Seoul National University
Kisoon Dan

Abstract

Discovery and verification of blood-based protein biomarker candidates for prediction of acute graft-versus-host disease and non-relapse mortality by using mass spectrometry-based proteomics approaches

Kisoon Dan
Department of Clinical Medical Sciences
The Graduate School
Seoul National University

Graft-versus-host disease (GVHD) is a major complication of allogeneic hematopoietic stem cell transplantation (allo-HSCT), which is a treatment for different types of malignant and non-malignant hematological disorders. Clinically, acute GVHD (aGVHD) represents a critical barrier to widespread utilization of alloHSCT as a first-line therapeutic option despite its unique curative potential because it is a major cause of non-relapse mortality (NRM) in patients undergoing alloHSCT. Biomarkers for predicting the risk of aGVHD can be used to identify, before the onset of clinical manifestation, high-risk patients who may benefit from early risk-reducing interventions such as

preemptive immunosuppressive therapy. Efforts have also been made to identify markers for predicting aGVHD development before the onset of clinical symptoms. However, no single biomarker or composite panel has been established to clearly discriminate between patients who will develop aGVHD and those who will not.

In this study, I investigated potential biomarkers for predicting the risk of aGVHD and NRM using a label-free quantitative mass spectrometry-based proteomic method to identify candidate proteins as biomarkers and then verified the candidates by multiple reaction monitoring (MRM) mass spectrometry using plasma samples collected from patients who underwent allHSCT. In the discovery phase, I compared the proteome profile of pooled plasma obtained from 5 aGVHD-positive patients and 5 aGVHD-negative patients. A total of 202 unique proteins was identified in the two groups. Among them, 16 differentially expressed proteins (DEPs) predicted to be associated with aGVHD development were extracted and subjected to MRM MS-based relative quantification. Thirty-four heavy peptides were used for MRM method development, and the established liquid chromatography (LC)-MRM method was applied to measure the relative protein levels in individual patient samples (n = 10) used in the discovery experiments. Seven candidate proteins with significantly higher levels in the GVHD-positive patient group (beta-2—microglobulin, leucine-rich alpha-2-glycoprotein, epidermal growth factor-containing fibulin-like extracellular matrix protein 1, peroxiredoxin-2, metalloproteinase inhibitor 1, plastin-2, and REG 3α) were subjected to MRM

MS-based absolute quantification for verification of the method in an independent patient cohort. A total of 88 multiplexed MRM transitions were established and applied to precisely measure the absolute concentration of 14 candidate peptides in the plasma of 89 patients.

The predictive value of the candidate biomarkers was evaluated in terms of the risk of aGVHD and NRM by constructing an optimal multivariable Cox model containing clinical characteristics and biomarker candidate levels as variables. Patients with high levels of each candidate biomarker showed a consistent tendency towards a higher risk of aGVHD and NRM, as compared to patients with low levels of these markers in the post-engraftment plasma samples of the verification set. TIMP-1, plastin-2, and REG3α were selected and used together to develop a biomarker panel score that ranged from 0 to 3. The biomarker panel score was significantly correlated with the risk of aGVHD and NRM in the univariable and multivariable Cox models. Model performance evaluation based on likelihood ratio test, five-fold cross-validated C (5-CVC) indices, and a continuous form of the survival-based net reclassification improvement (NRI) index demonstrated that addition of the biomarker panel score to clinical predictors significantly improved the discriminatory performance of the Cox model for predicting aGVHD risk and NRM. These findings suggest that plasma-based protein biomarkers can be used to predict aGVHD occurrence and NRM before the clinical onset of symptoms.

Keywords

Graft-versus-host disease, Allogeneic hematopoietic stem cell transplantation, Proteomics, Mass spectrometry, Liquid chromatography-mass spectrometry, Biomarker discovery, Biomarker verification

Student Number: 2014-30909

List of Tables

List of Figures

List of Abbreviations and Symbols

2D: Two dimensional

ABC: Ammonium bicarbonate

AGVHD: Acute graft versus host disease

AIC: Akaike information criterion

AlloHSCT: Allogeneic hematopoietic stem cell transplantation

BM: Bone marrow

CE: Collision energy

CI: Confidence interval

CV: Coefficient of variation

CVC: Cross-validated Harrell's C

DEP: Differentially expressed protein

DTT: Dithiothreitol

DW: Distillated water

HLA: Human leukocyte antigen

HPLC: High performance liquid chromatography

HR: Hazard ratio

IAA: Iodoacetamide

ID: Internal diameter

KM: Kaplan-Meier

LOD: Limit of detection

LOQ: Limit of quantification

M/Z: Mass-to-charge ratio

MRM: Multiple reaction monitoring

MS: Mass spectrometry/spectrometer

NRI: Net reclassification improvement

NRM: Non-relapse mortality

PAR: Peak area ratio

PBSC: Peripheral blood stem cells

RMS: Root mean square

SDS-PAGE: Sodium dodecyl sulfate polyacrylamide gel electrophoresis

TFA: Trifluoroacetic acid

Table of Contents

1. Introduction

Allogeneic hematopoietic stem cell transplantation (alloHSCT) is a cornerstone in the treatment of many malignant and non-malignant hematological disorders and genetic diseases, often providing the only chance of a cure. Although the transplanted allogeneic immune system has additional therapeutic benefits such as graft-versus-leukemia effect in malignant diseases including acute myeloid leukemia (AML) and acute lymphoblastic leukemia (ALL), in approximately half the recipients it is unavoidable that donor lymphocytes also recognize and attack normal host tissue, particularly the skin, liver, and gastrointestinal tract, causing acute graft-versus-host disease (aGVHD) [1]. Clinically, aGVHD represents a critical barrier to widespread utilization of alloHSCT as a first-line therapeutic option despite its unique potential for curing disease because it is a major cause of non-relapse mortality (NRM) in patients undergoing alloHSCT [2]. Although considerable advancements have been made in the understanding of its pathophysiology, treatment for aGVHD has only minimally changed over the last several decades. Therapeutic approaches have been nearly uniform for most patients over the past several decades, with high-dose systemic corticosteroid as the only reliable first-line treatment choice (2). Although corticosteroid alone shows an approximately 50% rate of symptomatic resolution, the remaining patients are at risk of developing steroid-refractory aGVHD for which no consensus exists regarding optimal management [3]. Steroid-refractory GVHD is a major therapeutic challenge and associated with poor prognosis. Therefore, individualized treatment based on the risk of developing advanced-stage aGVHD, treatment resistance, and transplant-related mortality (TRM) is essential for improving patient outcomes. Many researchers have attempted to develop reliable and easy-to-implement risk-stratifying measures incorporating both clinical characteristics and aGVHD-specific biomarkers [4].

Identification of GVHD-specific biomarkers from readily obtainable samples in the clinic such as peripheral blood or urine have been the most actively investigated subject in recent GVHD research. GVHD-specific biomarkers may be clinically useful, as diagnosis of aGVHD solely based on symptoms and signs is nonspecific and typically requires biopsy of the involved organ, an invasive procedure with a risk of complications. Previous studies mainly focused on the discovery of diagnostic biomarkers and assessing their value for discriminating patients with active aGVHD versus controls [5]. Numerous markers have been reported to be associated with not only aGVHD diagnosis itself, but also the eventual severity, treatment response, and non-relapse mortality [6-9]. Although these markers have not been validated in the clinical trial setting, they are attractable candidates for identifying patients who are likely to benefit from more intensive immunosuppression or molecular target-based therapy [10].

Although more difficult to achieve, efforts have also been made to identify markers for predicting aGVHD development before the onset of clinical symptoms [11, 12]. Because aGVHD is a major source of morbidity and NRM after alloHSCT, biomarkers useful for predicting the risk of aGVHD can allow identification of high-risk patients before the onset of clinical manifestation; these patients may benefit from early risk-reducing interventions such as preemptive immunosuppressive therapy. However, in contrast to the positive results of diagnostic biomarker studies, no single biomarker has been established to clearly discriminate between patients who will develop aGVHD and those who will not. A composite panel consisting of the three most plausible biomarker proteins showed only 57% sensitivity and 75% specificity in prediction, indicating much poorer reliability than other highly accurate diagnostic candidate marker panels [13]. Therefore, it is necessary to discover and verificate new predictive biomarkers that can be utilized to predict not only aGVHD development but also NRM.

Recent advances in mass spectrometry-based qualitative and quantitative proteomic techniques have enabled the discovery of protein candidate biomarkers and made verification more efficient and feasible using complex clinical samples such as plasma, urine, and tissue [14 -17]. Candidate biomarker from discovery proteomics experiment should be verified using precise and reproducible analytical methods. A preclinical verification process is essential for translating biomarker discoveries to clinical use [18]. For this purpose, mass spectrometry-based targeted proteins quantification technologies such as multiple reaction monitoring (MRM) have been proposed and developed. Enzyme-linked immunosorbent assays, still standardized methods for clinical verification and validation of candidate biomarkers, require the development of highly specific antibodies, which are sometimes difficult to produce and not well-suited for quantitating large numbers of candidate protein biomarker in the preclinical verification phase [19]. MRM methods do not require an antibody development process, but rather surrogate peptides, which are relatively easy to develop and can be used to quantify any protein in a clinical sample [20]. This technique has been standardized over the past 10 years and was demonstrated to be a precise complementary analytical method for protein quantification in a multiplexed manner for pre-clinical verification in numerous biomarker studies. [21-25].

Based on this theoretical background, I investigated potential protein biomarkers for predicting the risk of aGVHD and NRM using a label-free quantitative mass spectrometry-based proteomic method to discover candidate protein biomarkers followed by verification of discovered candidates by MRM mass spectrometry in prospectively collected independent peripheral blood samples of patients who underwent alloHSCT.

2. Materials and Methods

2.1. Reagents and chemicals

All reagents were American Chemical Society-grade or higher. All solvents used, including water, acetonitrile, and methanol, were liquid chromatography (LC)-mass spectrometry (MS)-grade and acquired from Fisher Scientific (Waltham, MA, USA). Chemicals (e.g., ammonium bicarbonate, iodoacetamide) and reagents (e.g., formic acid, trifluoroacetic acid (TFA)) were obtained from commercial sources at the highest purities available. Ammonium bicarbonate (ABC) solution was purchased from Sigma-Aldrich (St. Louis, MO, USA). Iodoacetamide (IAA) and dithiothreitol (DTT) was purchased from Sigma-Aldrich. RapiGest surfactant (SF) was purchased from Waters Corp. (Milford, MA, USA). Sequencing-grade chymotrypsin was purchased from Promega (Madison, WI, USA). Unpurified and highly purified isotope-labeled standard peptides (30–70%, >90% purity, respectively, according to the manufacturer) were obtained from JPT Peptide Technologies (Acton, MA, USA).

2.2. Sample collection and study design

This study was conducted with approval from the Institutional Review Board (IRB) of the Seoul National University Hospital (IRB protocol number, 1306-093-499). All patients or their legal guardians provided written informed consent for plasma sample collection. All procedures were carried out in accordance with the Helsinki Declaration (revised in 2013; World Medical Association). Eligible patients were retrospectively identified from a registry including patients with benign or malignant hematological disorders who underwent the first alloHSCT from 2005 to 2011 at Seoul National University Hospital (SNUH) and provided written informed consent for plasma sample collection. Patients who received prior alloHSCT were excluded. Donor and recipient

HLA-A, -B, -C, -DRB1, and -DQ allele types were determined at high resolution before unrelated donor transplantation, while related donors were evaluated for HLA-A, -B, -C, and -DRB1 at a minimum of intermediate resolution. GVHD prophylaxis was administered to all patients depending on the donor type, HLA match status, conditioning regimens, and tolerance to each prophylactic agent. Specifically, all patients were intravenously administered a calcineurin inhibitor predominantly cyclosporine A) starting on day -2. Methotrexate was intravenously administered starting on day 1 when the donor was HLA-mismatched. Mycophenolate was used rather than methotrexate in methotrexate-intolerant patients. Anti-thymocyte globulin was administered from day -3 to -1 intravenously for select conditioning regimens (reduced-intensity busulfan plus fludarabine, nonmyeloablative busulfan plus fludarabine, cyclophosphamide plus fludarabine, and melphalan plus fludarabine). aGVHD was diagnosed clinically with histologic confirmation when appropriate. Grading was based on the modified Glucksberg criteria (26). Data regarding patient characteristics and transplant-related outcomes were obtained from medical records. All patients in the registry provided plasma samples at the beginning of conditioning chemotherapy, on the day of stem cell infusion, and weekly thereafter until discharge or death. Ten milliliters of peripheral blood were centrifuged at 3,000 ×g for 5 min at 4°C to pellet debris. The resulting supernatant was aliquoted into in volumes of 1 mL and stored at - 80°C.

2.3. Sample preparation for discovery of biomarker candidates

Peripheral blood samples from patients who received alloHSCT were taken at the time of clinical diagnosis of GVHD and no GHVD with a median of 15 days after alloHSCT. Stored plasma samples from 5 alloHSCT patients presenting with GVHD and 5 alloHSCT patients presenting with no GVHD were thawed on ice and centrifuged at 3,000 *g* for 5 min at 4°C. Then, supernatant were pooled with same volume respectively,

making two pooled plasma samples. Characteristics of patients for discovery set are shown in Table 1. Thirty μL of pooled plasma was diluted 1:4.with buffer A (Agilent Technologies, cat no: 5185-5987) and passed through 0.22 μm spin filters (Agilent Technologies, cat no: 5185-5990). 14 high-abundance human plasma proteins (albumin, IgG, IgA, transferrin, α1-antitrypsin, and haptoglobin, fibrinogen,α2-macroglobulin, α1-acid glycoprotein, apolipoprotein A-1, apolipoprotein A-2, IgM, transthyretin, and complement C3) was removed from each filtered plasma sample by the MARS 14 immunoaffinity column (multiple affinity removal system, Hu-14 HC, 4.6 × 100 mm; Agilent, cat no: 5188-6558). Flow-through fraction was collected manually and was transferred to sample tube for concentration. Plasma depleted of high-abundant proteins were concentrated by centrifugal filtration using a 0.5 mL of 3,000 Da molecular weight cutoff (MWCO) filter (Amicon® Ultra 3K, Millipore, cat no: UFC500324) according to manufacturer's protocol. Buffer exchanging of concentrated plasma with 50 mM ammonium bicarbonate was done using same centrifugal filter. Buffer exchanged and concentrated plasma protein was quantified by Bradford assay (Quick Start Bradford Protein Assay kit (BioRad, cat no: 500-0207).

2.4. SDS-PAGE and in-gel trypsin digestion

The concentrated proteins were mixed with 4x Laemmli sample buffer and 2-mercaptoethanol mixture solution (cat no: 161-0747, 161-0710, respectively; Bio-Rad) and heated for 5 min at 95°C. Next, 40 μL of sample representing 30 μg of plasma proteins of each sample were loaded into a 4_20% Mini-PROTEAN® TGX™ Gel (cat. no. 456-1094; Bio-Rad) and electrophoresed at 100 V. Separated proteins were stained with Bio-Safe Coomassie Stain (cat. no. 161-0786; Bio-Rad) for 90 min according to the manufacturer's protocol. Each gel lane per sample was sliced into 8 slices using a razor blade, and each sliced gel was washed twice with 25 mM ABC and destained with 50% acetonitrile in 100 mM ABC solution. After dehydration with a vacuum

concentrator (Savant™ SPD2010, SpeedVac™, Thermo Scientific), each gel slice was treated with 20 mM DTT and incubated at 56℃ for 30 min. The gel slices were treated with 100 mM iodoacetamide and incubated in the dark for 30 min at room temperature (21-22℃). After sequential treatment with 50 mM ABC and 100% acetonitrile with vortexing, the gel slices were dried in a vacuum concentrator. The dried gel slices were treated with 400 ng of sequencing-grade modified trypsin solution (Promega) and incubated at 37°C overnight. After transferring the supernatant solution into a new tube, the remaining peptides were extracted from the gel slices by a treatment with 4% formic acid in 98% distillated water, sonicated for 3 min, followed by treatment with 4% formic acid in 80% acetonitrile, and further sonication was conducted for 3 min. The digested peptides were pooled and dried in a vacuum concentrator.

2.5. Peptides separation with two dimensional (high/low pH) reverse phase NanoLC

Digested and dried peptides was reconstituted in 80 mM ammonium formate and 4 μL of sample was used for analysis. Nanoscale LC separation of tryptic peptides was performed using a nanoAcquity™ UPLC® system with online 2D (Reverse-phase/Reverse-phase) Technology (Waters Corp.) equipped with two nano-binary solvent pumps. The digested and dried peptide samples were reconstituted in 12 μL of 80 mM of ammonium formate (pH 9.8), and 5 μL of samples were injected and trapped in the first trapping column (XBridge™ BEH C18, 5 μm, 300 μm × 50 mm; Waters Corp.) at a flow rate of 2.0 μL/min with 97:3 (v:v) of eluents (A: pH 9.8, 20 mM of ammonium formate in water, B: acetonitrile). Peptides were eluted from the first trapping column by a discontinuous step gradient containing acetonitrile (10.8%, 14.0%, 16.7%, 20.4%, and 65.0%), typically for 5 fractions. Eluted peptides from the first-dimension trapping column with the discontinuous step gradient of acetonitrile

were moved to the mixing tee (Dilution Tee) and mixed with 99:.1 (v/v) of mobile phase (A: 0.1% formic acid in water, B: 0.1% formic acid in acetonitrile) at a flow rate of 20 μL/min using another LC pump. This 20-fold online dilution process in the mixing tee changes the pH of the eluent from 10 to 2.6 and reduces the acetonitrile composition, effectively enabling the peptides to be retained on the second trapping column. Peptides in low pH (2.6) solution and the diluted eluent were retrapped in the second-dimension trapping column (Symmetry C18, 5 μm, 180 μm × 20 mm, Waters Corp.). After trapping the sample on the second trapping column, the peptides were separated on an analytical column (BEH C18, 1.7 μm, 75 μm × 150 mm, Waters Corp.) with a linear gradient of 2–45% of mobile phase B over 90 min at a flow rate of 300 nL/min. The temperature of the analytical column was maintained at 40℃. This entire process involving trapping of peptides in high pH, dilution of pH and acetonitrile concentration, retrapping, and separating the peptides at low pH were repeated automatically according to total number of fractions programmed in the LC method until the end of the run. In my study, 5–10 fractions of peptides with 2D nanoLC were acquired per gel slice, depending on the complexity of the peptides. A total of 60 fractions was acquired per each pooled plasma sample.

2.6. Mass spectrometry data collection

Mass spectrometric analysis of tryptic peptides separated by 2D nanoLC was performed using a quadrupole time-of-flight mass spectrometer (SYNAPT MS, Waters Corp.) equipped with the nanoelectrospray ionization source. The time-of-flight analyzer of the mass spectrometer was externally calibrated with a b+ and y+ fragment ion series of [Glu1]-fibrinopeptide B. The mass spectrometer was operated in electrospray ionization positive ion mode with a typical resolution of 10,000 full width at half maximum. MS data were acquired in the continuum mode over an m/z range of 50–1,990 using a capillary voltage of 2.88 kV, source temperature of 80°C, and cone

voltage of 30 V. A multiplexed data acquisition method (MS^E) was used for mass spectrometric analysis [27]. The LC-MS^E data were collected by alternating the collision energy of the MS instrument every 1 s without precursor ion selection. In low-energy MS mode, the data was collected at a constant collision energy of 5.3 eV, while in MS^E mode, the collision energy was increased from 15 to 42 eV. A solution of 400 fmol/µL of [Glu1]-fibrinopeptide B in 30% acetonitrile with 0.1% formic acid was used as a lock-mass solution and sprayed from another nano-sprayer source at a frequency of every 30 s for accurate mass correction.

2.7. Data processing for protein identification and quantifications

Raw data was acquired in MS^E mode and processed with ProteinlynxGlobalServer 2.4 (Waters Corp.) to create processed spectra (peak lists) which have deisotoped, deconvoluted, and aligned precursor (MS) ions and their fragment ions (MS/MS) list based on similar retention times. Processed spectra (peak lists) containing precursor and time-aligned their fragment ions spectra were searched against the reviewed entries of Uniprot human protein database (Swiss-Prot, 2013_Mar, 20216 protein entries in total) databases using PLGS 2.4, which uses the embedded physicochemical properties of polypeptide and statistical models [28]. Search parameters used for protein identification included automatic peptide and peptide fragment ion tolerance settings (typically 10 and 20 ppm for precursor and fragment ions, respectively), one trypsin missed cleavage, carbamidomethylation on cysteine for fixed modification, deamidation on asparagine residues, oxidation on methionine for variable modification, and with a 2% of false-positive discovery rate at the protein level. We employed a label-free quantification approach to allow for simultaneous protein identification and quantification of proteins in complex plasma samples. Briefly, the average MS signal response of the three most abundant peptide ions to a specific protein were correlated with peptide ion signals of an internal standard protein that was spiked into the sample

at a known concentration. The presence of an internal standard proteins enables calculation of the molar response factor (instrument specific). The molar concentrations of each identified protein in a sample were subsequently determined by comparing the calculated average intensities of the three most abundant identified peptides with the molar response factor [29, 30]. We used ADH tryptic digest (alcohol dehydrogenase 1 (P00330), *Saccharomyces cerevisiae*, Waters Corp.) to determine the molar response factor for our MS instrument.

2.8. Sample collection and selection criteria for verification of target proteins

Sample collection was performed using the same method employed for discovery proteomics. To ensure the comparability of patients and clinical utility of identified proteins as predictive biomarkers, we used the following eligibility criteria to form the patient cohort for biomarker candidates verification: (1) successful engraftment within 28 days of alloHSCT and (2) no clinical onset of aGVHD manifestation before the engraftment day.

Engraftment was defined as the first of three/consecutive days with absolute neutrophil count ≥500/μL after alloHSCT. The engraftment day was defined as the first day when engraftment was confirmed (last day of three consecutive days). In total, 91 patients met these criteria. Plasma samples from these patients obtained on the engraftment day or later, but not later than the onset of aGVHD, were used to measure biomarker levels using the LC-MS MRM procedure for absolute quantification. Because two patients had no plasma samples obtained within this timeframe, these patients were excluded, leaving 89 patients in the verification set. As the plasma samples were collected at 1-week intervals, most patients had multiple samples fulfilling these criteria. Therefore, plasma samples obtained at the nearest date to

engraftment were selected to minimize sampling day bias.

2.9. Plasma sample preparation for verification of target proteins

Plasma samples were thawed on ice and centrifuged at 3,000 ×*g* for 5 min at 4°C. Supernatants were transferred into sample tubes (Protein Lobind, Eppendorf, Hamburg, Germany) and vortexed. Thirty microliters of each plasma sample were diluted by 1:1.37 in buffer A and passed through 0.22-µm spin filters (cat no: 5185-5990; Agilent Technologies). The process used for discovery proteomics was applied to deplete 14 high-abundant proteins. An infinity 1260 BioLC and automated fraction collector was used to collect the flow-through fraction automatically based on the UV detector signal response of proteins. Plasma depleted of high-abundant proteins samples were concentrated and buffer-exchanged using same process applied to discovery proteomics. Equal volumes of each plasma proteins were denatured with RapiGest™ surfactant (cat no: 186001861; Waters Corp.) for 20 min at 80°C. Denatured proteins were reduced by adding 50 mM dithiothreitol (Merck, Darmstadt, Germany) in 50 mM ABC at 60°C for 30 min and alkylated by adding 150 mM iodoacetamide (Sigma) at room temperature for 30 min in the dark. Sequencing-grade modified trypsin was added to plasma samples at a 50:1 plasma proteins substrate: trypsin ratio. High-purity stable isotope-labeled heavy peptides were mixed with the plasma samples just before adding trypsin. Digestion was carried out for 16 h at 37°C. Tryptic digestion was quenched by addition of 1% TFA at a final concentration of 0.5% (v/v) and incubation for 45 min at 37°C. Samples were then centrifuged for 10 min at 15,871 × *g* at 4°C to pellet RapiGest and undigested proteins. The sample supernatant was desalted and concentrated by solid-phase extraction using the OASIS HLB desalting cartridges (cat no: WAT094225, Waters Corp.). The Oasis cartridge was washed sequentially with a total volume of 3 mL of 0.1% TFA acid in acetonitrile and equilibrated with 3 mL of 0.1% TFA in water.

Samples were then loaded onto desalting cartridges and the cartridges were washed with 3 mL of 0.1% TFA and eluted with 0.4 mL of 0.1% TFA in 80% acetonitrile. The eluted peptides were lyophilized on a speed vacuum centrifuge (CcntriVap® centrifugal concentrator, LABCONCO, Kansas City, MO, USA), and stored at -80°C until use. Prior to LC-MRM/MS analysis, the samples were reconstituted in 20 µL of 0.1% formic acid in 1% acetonitrile and mixed with crude (purity unknown) stable isotope-labeled heavy peptides.

2.10. Peptides separation and MRM MS data acquisitions for verification

The Agilent 1260 Infinity capillary flow HPLC system was used to inject 5 µL of digested plasma protein sample (reconstituted in 20 µL of 0.1% formic acid in 1% acetonitrile) onto a reversed phase analytical column (ZORBAX SB-C18, 3.5 µm, 150 mm in length, 0.5 mm in I.D; Agilent Technologies). The temperature of the separation column was maintained at 40°C. Peptides separation was conducted at a flow rate of 20 µL/min on a linear gradient of mobile phase B (0.1% formic acid in acetonitrile) from 2% to 45% over 55 min. The total run time was 80 min (mobile phase A: 99.9%/0.1% v/v, water/formic acid, mobile phase B: 99.9%/0.1% v/v, acetonitrile/formic acid). A triple quadrupole LC/MS system (6495 LCMS, Agilent Technologies) was used for detection of m/z and signal intensity of eluted peptides from the separation column. Automated optimization of electrospray source parameters and mass axis calibration in electrospray ionization-positive mode were conducted automatically using the autotune function in MassHunter Workstation software (ver B.08.00, Agilent Technologies) with tuning solution (G1969-85000, Agilent Technologies). MRM-MS analysis was conducted in positive ion mode with the ion spray capillary voltage and nozzle voltage at 3000 and 1000 V, respectively. The drying gas temperature was set to 250°C at a flow rate of 15 L/min, while the sheath gas temperature was set to 300°C at a flow rate of 12 L/min. Nebulizer gas flow was set at

30 psi, Delta electron multiplier voltage was set to 300 V, and cell accelerator and fragment voltages were set at 5 and 380 V, respectively. Resolution of MS quadrupole-1 and quadrupole-3 was set to unit resolution (0.7 full width at half maximum). Dynamic scheduled MRM-MS acquisition methods were constructed for efficient multiplexed MRM-MS data acquisition using retention time and collision energy information from each MRM transition. The target cycle time for MRM-MS methods of relative quantification was set to 700 ms for a total of 166 MRM transitions and for the MRM-MS method of absolute quantification was set to 450 ms for a total of 88 MRM transitions maintaining a minimum dwell time of 5 ms. The min/max dwell times were adjusted automatically depending on the number of concurrent transitions with MassHunter Workstation software. The retention time tolerance window for dynamic scheduled MRM-MS methods was 4 min.

2.11. MRM data processing and method development for target protein quantification

Skyline software (ver.3.6, University of Washington, Seattle, WA, USA) [31] was used to build quantifiable target peptides and transition lists from 10 differentially expressed proteins (DEPs). FASTA-formatted primary amino acid sequences of 10 DEPs were imported to create target peptides list with the following conditions. 1) *In silico* tryptic (KR|P) digestion with no miscleavage, 2) restricted length of tryptic peptides ranging from 6 to 25 amino acids, and 3) peptides containing methionine or a possible glycosylation site (NXT/NXS) and RP/KP were excluded. Filtering conditions for MRM transitions were constructing doubly or triply charged precursor ions, singly or doubly charged fragment ion, and monitoring for both y and b fragment type ions. The final target peptide selection for MRM method development was conducted with following criteria. 1) Firstly, peptides identified from discovery experiments were

selected, 2) high-confidence peptides (mostly higher MS and MS/MS intensity), 3) Some target peptides that were not identified in our discovery experiment but present in the SRM (www.srmatlas.org) or PeptideAtlas (www.peptideatlas.org) database were added to maintain the number of target surrogate peptides as 3 and more as possible at the initial stage of method development. All integrated peaks by Skyline were manually inspected to confirm correct peak detection and integration, and incorrectly integrated peaks were manually corrected.

MRM-MS acquisition methods were initially built with 8–12 light (endogenous peptides) and heavy (stable isotope-labeled peptides) transitions per peptide. Characteristics of MRM transitions for each heavy peptide including retention time, optimized collision energy (CE), MS signal intensity, and interference were inspected in the plasma protein digest used as a matrix spiked with heavy peptides. We reviewed the MRM data to refine transitions showing better MS responses, no interference, and consistent signal intensity over consecutive LC-MS runs. Target peptides that did not meet the following criteria were excluded during method development: 1) very low light and heavy peptide MS response and 2) peptides failed to build up 3 or above transitions detected reproducibly and free of interference from the plasma matrix. The final MRM method was composed of 3–4 refined transitions per each peptide. The peak area ratio, which refers to the ratio of the integrated peak area of the light peptide to the integrated peak area of the corresponding heavy peptide was used to calculate the relative abundance of each peptide. The absolute concentration of each peptide was calculated by multiplying the spiked heavy peptide concentration to peak area ratio. The calculated concentration is reported in terms of μg/mL of plasma.

2.12. Establishment of response curve and absolute quantification with MRM methods in verification cohort

A reverse response curve was generated with 8 plasma matrix samples with heavy peptides plus 1 plasma matrix sample without heavy peptides, based on nine samples containing equal amounts of tryptic digest of plasma proteins as a background matrix. Heavy peptides were spiked into the tryptic digest of plasma proteins and then serially diluted (2x), covering a 128-fold concentration range. MRM data for each calibration point was acquired three times. Spiking concentrations of heavy peptides to the background matrix were adjusted to the peak areas of corresponding light peptides so that the light to heavy peptide peak area ratio ranges between 0.1 to 10. Blank runs of tryptic digest of plasma proteins without heavy peptides provided estimates of chemical background levels. QUASAR [32] was used to create plots of MS response versus known concentration of the 8-point MRM data and evaluate the linearity of the measurements across the range of spiked heavy peptide concentrations for each MRM transition. The limit of quantification (LOQ) and limit of detection (LOD) were determined at defined signal-to-noise ratio (S/N) values. The LOD was determined as the average of background values from three blank runs plus the standard deviation of background values multiplied by three. The LOQ was determined as the average of background values from three blank runs plus the standard deviation of background values multiplied by ten [33]. In my study, we defined the lower LOQ (LLOQ) as the functional sensitivity determined as the lowest concentration point with a coefficient of variation (CV) below 20% in the response curve. Functional sensitivity was used as an LLOQ in this study. CV criteria for the other concentration points above the LOQ had a CV below 20%. The upper LOQ (ULOQ) was defined as the highest concentration point of each peptide that had a CV below 20%.

Established multiplexed MRM methods were applied to measure the absolute levels of target peptides in individual plasma samples from a total of 89 patients. Two technical replicate LC-MS runs were conducted in randomized injection order. The calculated concentration value with each peak area ratio (PAR) and known concentration of heavy peptides was converted to units of μg/mL of plasma, and those of two technical replicates were averaged. One best transition (named as the quantifier) which showed the lowest functional sensitivity, good linearity, and no interference was selected for absolute quantification.

2.13. Statistical analysis

Correlation analysis, creation of the scatter diagram, and nonparametric Mann Whitney test was conducted using MedCalc Statistical software (ver 17.7.2, Ostend, Belgium) to compare the linear relationships of pairs of surrogate peptides from the same proteins. Spearman correlation coefficients were used for correlation analysis. Log-transformed concentration values were used for data with wide concentration range.

In the verification set, univariable Cox proportional hazards regression analysis was first performed for all potential clinical predictors and each candidate biomarker to assess the association between these variables and the risk of aGVHD and NRM. Next, we used a two-step exhaustive screening procedure to construct optimal multivariable Cox proportional hazard regression models (Cox models) to predict the risk of aGVHD and NRM [34]. First, we selected the best subset of clinical covariates to include in the multivariable model. Second, by adjusting for the selected clinical predictors, we identified the best combination of biomarkers for predicting the risk of aGVHD and NRM separately. The optimal model was defined by the lowest Akaike Information Criterion value among the models containing all possible combinations of input variables. Using the identified combination of biomarkers, we defined the biomarker

panel score as the number of protein markers showing a high level in a given patient. This score was used as a continuous variable to assess the collective effect of biomarker levels on the risk of aGVHD and NRM in subsequent analyses.

We examined increasing the value of model performance by adding the biomarker panel score to the clinical predictors based on the likelihood ratio test, five-fold cross-validated Harrell's C (5-CVC) indices, and a continuous form of the survival-based net reclassification improvement (NRI) index [35,36]. To determine the distribution of the 5-CVC indices, we repeated random splitting of the dataset into five groups and calculated 5-CVC 200 times for each model. Student's *t*-test was used to compare the 5-CVC between the model incorporating clinical predictors only and that incorporating clinical predictors plus the biomarker panel score. NRI calculation was based on 6-month Kaplan-Meier estimates for the risk of aGVHD and 1-year Kaplan-Meier estimates for NRM. The percentile bootstrap method was used to estimate the 95% confidence interval (CI) and determine the statistical significance of NRI. As a supplementary analysis, we assessed the predictive value of each candidate biomarker level for the risk of aGVHD and NRM independently of the clinical characteristics using the same variable selection algorithm described above.

The difference in cause-specific hazards may not directly translate to the difference in the actual incidence. Therefore, I estimated the cumulative incidence of aGVHD and NRM using the cumulative incidence function and compared this value between groups using Gray's test [37]. Death without aGVHD and relapse were considered as competing risks of aGVHD and NRM, respectively. Finally, we developed Fine-Gray subdistribution hazards regression models (Fine-Gray models) to evaluate the predictive value of the biomarker panel score in determining the actual incidence of aGVHD and NRM [38]. All tests were two-tailed. Differences were considered significant at a P value of less than 0.2 in the discovery proteomic analysis and a P value

of less than 0.05 in the verification set analysis. R version 3.5.0 (R Foundation for Statistical Computing, Vienna, Austria) was used for computation. Our LC-MS MRM procedure quantified two peptides corresponding to each candidate protein biomarker, and the levels of all peptide pairs showed high correlations (Pearson correlation coefficient > 0.97, Figure 4). Therefore, we averaged the levels of two peptides from the same protein to obtain protein-level values. Each protein marker level was logarithmic-transformed and dichotomized at the median to classify patients into 'high' and 'low' level groups.

Table 1. Overview of characteristics of patients for discovery study

	Sex	Diagnosis	Age	Conditioning Regimen	Acute GVHD onset day	Sampling day	Type of GVHD		
							Skin	Liver	GI
1	F	ABL[c]	31	BuCy	D[a] 20	D21	2[b]	2	0
2	F	ALL[d]	24	BuCy	D8	D14	1	1	1
3	M	AML[e]	27	MelFlu	D12	D14	1	2	1
4	F	AML	16	BuCy	D5	D15	1	0	0
5	F	MDS[f]	51	BuCy	D20	D22	1	0	0
6	F	MDS	42	BuCy	N/A	D14	0	0	0
7	M	ALL	33	BuCy	N/A	D21	0	0	0
8	F	ALL	27	BuCy	N/A	D14	0	0	0
9	M	AML	56	MelFlu	N/A	D14	0	0	0
10	F	AML	33	BuCy	N/A	D14	0	0	0

a : 'D' indicates day of alloHSCT (D 20 : 20 days after alloHSCT)
b : number denotes clinical grade of GVHD (1 – 4), Grading of aGVHD was based on the modified Glucksberg criteria[26]
c: Acute biphenotypic leukemia d: acute lymphocytic leukemia e: Acute myelogenous leukemia
f: Myelodysplastic syndromes

3. Results

3.1. Strategy for discovery and verification of protein biomarkers candidates

To discover biomarker candidate for predicting acute graft-versus-host disease after alloHSCT, a label-free quantitative mass spectrometry-based proteomics method was applied. We compared the proteome profiles of pooled plasma samples obtained at a median of 15 days after alloHSCT from 5 patients with GVHD and without GVHD. Highly abundant proteins from the plasma were separated using a MARS-14 column and fractionated by SDS-PAGE. Each gel slice was in-gel digested, and the digested peptides were separated and quantitatively analyzed using 2D nanoLC (high/low pH) and quadrupole time-of-flight MS. After qualitative and quantitative data analysis, we generated a candidate biomarker protein list from the DEPs. Next, surrogate peptides from the candidate biomarker protein were selected for MRM quantification, and heavy peptides (stable isotope-labeled peptides) were purchased. An MRM method with crude heavy peptides was developed and applied to measure the relative amounts of candidate peptides from 10 individual patients used in the discovery phase. Based on these results, further candidate peptides selection was conducted and MRM methods development for absolute quantification with high-purity heavy peptides was established. I precisely measured amount of target candidate peptides in independent patient cohort (n = 89) using the established MRM method. The predictive value of the candidate biomarkers in terms of the risk of aGVHD and NRM was evaluated by constructing an optimal multivariable Cox model containing clinical characteristics and levels of biomarker candidates as variables. Figure 1 illustrates the workflow for discovery of biomarker candidates from the plasma and verification of the biomarker candidates in an independent patient cohort.

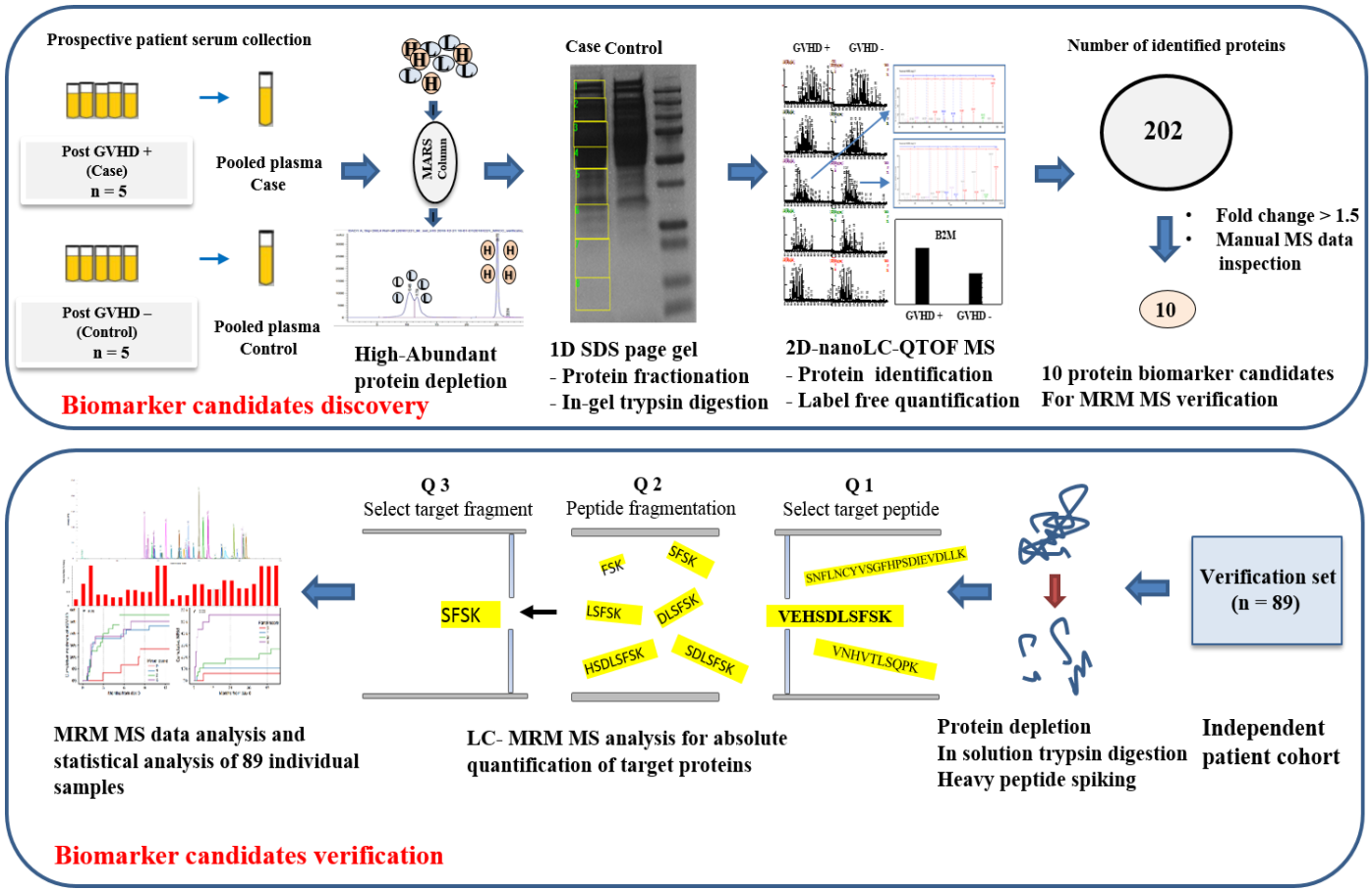

Figure 1. Workflow of biomarker candidates discovery and verification in independent patient cohort

3.2. Patient characteristics

Patient characteristics are summarized in Table 2 for the discovery and verification sets. The discovery set included two AML pairs, one ALL pair, one acute biphenotypic leukemia (ABL)-ALL pair, and one myelodysplastic syndrome (MDS) pair of patients. All patients were below the age of 60 years at the time of transplantation. Eight patients received myeloablative conditioining (MAC) with busulfan and cyclophosphamide (BuCy), while the remaining two AML patients received reduced-intensity conditioning (RIC) with fludarabine, melphalan, and antithymocyte globulin (FluMelATG). All patients in the verification set were below the age of 65 years at the time of transplantation. Two-thirds of the patients were diagnosed with acute leukemia, including 38 (42.7%) AML and 21 (23.6%) ALL, while 20 patients (22.5%) had benign hematological diseases including MDS (n = 7), primary myelofibrosis (PMF, n = 4), severe aplastic anemia (n = 6), paroxysmal nocturnal hemoglobinuria (n = 2), and hemophagocytic lymphohistiocytosis (n = 1). The most frequently used conditioning regimen was BuCy (n = 36), followed by nonmyeloablative FluBuATG (n = 30). The major source of stem cells was the peripheral blood in both cohorts. All patients received GVHD prophylaxis per protocol.

3.3. Selection of biomarker candidate proteins from DEPs list

A total of 202 unique proteins were identified in the two groups. Among them, we extracted DEPs showing more than 1.5-fold change based on the results of label-free quantification, with 21 proteins differentially expressed between the two groups. Sixteen proteins were more abundant in the GVHD group and 5 proteins were more abundant in the no-GVHD group (Table 3). Next, the MS and MS/MS data were manually inspected to remove poor MS and MS/MS data (mostly matched at low confidence levels), which may have been false-positive protein identifications using

the probability-based database search algorithm, to prevent incorrect quantitative results [39].

3.4. Establishment of multiplexed MRM method for relative quantification using heavy peptides

Among the 16 DEPs upregulated in the GVHD group, we selected 10 proteins corresponding to 34 proteotypic peptides for MRM verification method development. C-reactive protein was excluded from the verification target list because it is a nonspecific inflammatory marker that can be elevated in various inflammatory conditions. Table 4 shows the 34 surrogate peptides from 10 DEPs and their characteristic data identified during the discovery phase. A total of 34 heavy-isotope-labeled peptide standards (SpikeTides^{TM}, JPT Peptide Technologies) with unknown purity grade was purchased. To evaluate the suitability of the heavy surrogate peptides for MRM method development, we identified the retention time, optimized CEs, and MS signal response for heavy peptides by spiking the heavy peptides into the matrix plasma protein tryptic digest. Of the 34 heavy peptides, 20 were selected for relative quantification. Fourteen peptides were excluded because they did not meet the criteria (described in section 2.11). Eight to twelve MRM transitions for each peptide at the beginning of method development were monitored and refined as 3–6 MRM transitions per peptide throughout the method development process. We measured the relative amounts of target candidate peptides by applying the established MRM method to individual patient samples (n = 10) used in the discovery experiment and obtained each peak area ratio, which was expressed as the ratio of the light peak area to the heavy peak area. Mann-Whitney U test was conducted to compare the differences in the peak area ratio of each candidate protein (Table 5). A P-value of less than 0.20 was considered to indicate statistical significance for the differences between the two

groups. Seven candidate proteins met the criteria (P-value < 0.2): Beta-2—microglobulin, leucine-rich alpha-2-glycoprotein, epidermal growth factor-containing fibulin-like extracellular matrix protein 1, peroxiredoxin-2, metalloproteinase inhibitor 1, plastin-2, and REG 3α. A total of 14 peptides from 7 proteins were finally selected and used to develop an absolute MRM quantification method for verification in an independent large patient cohort.

Table 2. Patient characteristics

Characteristics	Discovery set (N = 10)	Verification set (N = 89)
Median age at alloHSCT (range), y	32 (16-57)	44 (16-64)
Sex, n (%)		
Male	3 (30)	53 (59.6)
Female	7 (70)	36 (40.4)
Diagnosis, n (%)		
AML/ALL	8 (80)	59 (66.3)
CML/MDS/PMF	2 (20)	12 (13.5)
Other malignant	0 (0)	9 (10.1)[a]
Other benign	0 (0)	9 (10.1)[b]
Conditioning, n (%)		
Myeloablative[c]	8 (80)	37 (41.6)
Reduced-intensity[d]	2 (20)	20 (22.5)
Nonmyeloablative[e]	0 (0)	32 (36)
Stem cell source, n (%)		
BM	1 (10)	8 (9)
PBSC	9 (90)	81 (91)
Donor relationship and HLA match, n (%)		
Related		
Full match	2 (20)	48 (53.9)
Haploidentical	0 (0)	3 (3.4)[f]
Unrelated		
10/10 match	6 (60)	17 (19.1)
9/10 match	2 (20)	16 (18)
8/10 match	0 (0)	5 (5.6)
Donor sex, n (%)		
Male	8 (80)	63 (70.8)
Female	2 (20)	26 (29.2)
Median donor age (range), y	32 (25-46)	37 (8-77)
GVHD prophylaxis, n (%)		
CNI	1 (10)	11 (12.4)
CNI + MTX	9 (90)	36 (40.4)
CNI + MMF	0 (0)	1 (1.1)
CNI + ATG	0 (0)	22 (24.7)
CNI + MTX + ATG	0 (0)	19 (21.3)

[a]Other malignant diseases include non-Hodgkin lymphoma (n = 7), aggressive NK cell leukemia (n = 1), and T-cell prolymphocytic leukemia (n = 1).

[b]Other benign diseases include severe aplastic anemia (n = 6), paroxysmal nocturnal hemoglobinuria (n = 2), and hemophagocytic lymphohistiocytosis (n = 1).

[c]Myeloablative conditioning regimens include BuCy and FluCyTLI.

[d]Reduced-intensity conditioning regimens include FluBuATG (fludarabine 30mg/m^2 × 6 days and busulfan 3.2mg/kg × 2 days), FluCyATG, and FluMelATG.

[e]Nonmyeloablative conditioning regimen includes FluBuATG (fludarabine 30mg/m^2 × 4 days plus busulfan 0.8mg/kg x 4 days).

[f]Haploidentical donors include one parent, one sibling, and one child of the respective recipients.

alloHSCT, allogeneic hematopoietic stem cell transplantation; AML, acute myeloid leukemia; ALL, acute lymphoblastic leukemia; CML, chronic myeloid leukemia; MDS, myelodysplastic syndrome; PMF, primary myelofibrosis; BM, bone marrow; PBSC, peripheral blood stem cell; GVHD, graft-versus-host disease; CNI, calcineurin inhibitor; MTX, methotrexate; MMF, mycophenolate mofetil; ATG, anti-thymocyte globulin.

Table 3. Deps list selected from all of the identified proteins in plasma between GVHD + and GVHD – groups

Uniprot accession number	Protein name	Fold change ratio (GVHD + to GVHD -)	Sequence Coverage* [%]	Number of identified peptide	Mol. weight [kDa]
P32119	Peroxiredoxin 2 EC 1 11 1 15	4.0	40.6	5	21.747
Q06141	Regenerating islet derived protein 3 alpha	3.4	37.6	4	16.555
P05109	Protein S100 A8	3.4	38.7	5	10.827
Q12805	EGF containing fibulin like extracellular matrix protein 1	2.7	27.5	11	52.730
P02792	Ferritin light chain	2.5	40.2	13	19.876
P07333	Macrophage colony stimulating factor 1 receptor	2.5	13.2	6	106.001
P02750	Leucine rich alpha 2 glycoprotein	2.4	64.7	56	34.325
P08571	Monocyte differentiation antigen CD14	2.4	40.4	14	37.991
P13796	Plastin 2	2.2	40.3	22	70.112
P02741	C reactive protein	2.1	31.6	40	23.032
P02749	Beta 2 glycoprotein 1	2.1	66.0	42	36.230
P00915	Carbonic anhydrase 1 EC 4 2 1 1	2.1	43.5	12	28.721
P61769	Beta 2 microglobulin	2.1	42.4	4	11.723
P01033	Metalloproteinase inhibitor 1	2.0	39.7	6	20.695
P02790	Hemopexin	1.9	84.1	112	49.263
P05451	Lithostathine 1 alpha	1.8	14.6	2	16.264
P04275	von Willebrand factor	0.5	28.8	68	306.821
P17936	Insulin like growth factor binding protein 3	0.4	35.2	7	28.731
P03951	Coagulation factor XI Short FXI EC 3 4 21 27	0.4	25.0	17	67.981
P00740	Coagulation factor IX EC 3 4 21 22	0.4	46.9	16	48.694
P20742	Pregnancy zone protein	0.2	11.9	16	160.954

*Sequence coverage: the percentage of the protein sequence covered by identified peptides

Table 4. Target peptides list for LC-MRM method development extracted from discovery proteomics result

Uniprot accession number	Protein name	Peptide sequence	Peptides identified in discovery experiments	Peptides present in human SRM or PeptideAtlas DB	Precursor ion mass error (ppm)	Score	Retention Time (min)	Intensity	Matched MS/MS ion list	MS/MS ion RMS mass error (ppm)
P05109	S100A8	ALNSIIDVYHK	O	O	0.97	8.01	64.83	21993	b4y2y3y4y5y6y7y8y9y11	11.01
P05109	S100A8	GNFHAVYR	N/A	O	N/A	N/A	N/A	N/A	N/A	N/A
P05109	S100A8	LLETECPQYIR	O	O	1.30	8.30	58.41	47741	b2b3b4b5b6b8b10b11y1y2y3y4y5y6y7y8y9y11	12.38
P05109	S100A8	GADVWFK	O	O	-3.43	7.06	62.68	4461	b6y1y2y3y4y5	11.88
P61769	Beta-2—macroglobulin	VEHSDLSFSK	O	O	-0.84	8.17	40.89	33131	b3b5b6b7y1y2y3y4y5y6y7y8y10	13.29
P61769	Beta-2—macroglobulin	HPAENGK	N/A	O	N/A	N/A	N/A	N/A	N/A	N/A
P61769	Beta-2--microglobulin	VNHVTLSQPK	O	O	0.77	7.21	34.08	13042	b3y2y5y6y7y10	4.81
P02750	Leucine-rich alpha-2-glycoprotein	TLDLGENQLETLPPDLLR	O	O	-1.14	9.01	91.29	870864	b2b3b5b8b9b11b12b13b18y1y2y3y5y6y7y8y9y10y13y16y18	10.59
P02750	Leucine-rich alpha-2-glycoprotein	LPPGLLANFTLLR	N/A	O	N/A	N/A	N/A	N/A	N/A	N/A
P02750	Leucine-rich alpha-2-glycoprotein	ENQLEVLEVSWLHGLK	O	O	-2.45	9.56	98.75	452612	b1b2b3b4b5b6b8b9b13b15b16y1y2y3y4y5y6y7y8y9y10y11y12y13y14y15y16	10.80
Q12805	EGF-containing fibulin-like extracellular matrix protein 1	EHIVDLEMLTVSSIGTFR	N/A	O	N/A	N/A	N/A	N/A	N/A	N/A
Q12805	EGF-containing fibulin-like extracellular matrix protein 1	NPCQDPYILTPENR	O	O	2.60	6.84	60.37	16203	b5y2y4y5y6y7y9y10y14	14.35
Q12805	EGF-containing fibulin-like extracellular matrix protein 1	DIDECDIVPDACK	O	O	1.44	7.48	60.53	19002	b4b6b7b8b9y2y3y5y6y7y9y10y13	10.56
Q12805	EGF-containing fibulin-like extracellular matrix protein 1	LNCEDIDECR	O	O	1.16	6.65	42.96	8426	y2y3y4y5y7y8y10	21.38

Table 4. Target peptides list for LC-MRM method development extracted from discovery proteomics result. Continued

Uniprot accession number	Protein name	Peptide sequence	Peptides identified in discovery experiments	Peptides present in human SRM or PeptideAtlas DB	Precursor mass error (ppm)	Score	Retention Time (min)	Intensity	Matched MS/MS ion list	MS/MS ion RMS Mass Error (ppm)
P32119	Peroxiredoxin-2	EGGLGPLNIPLLADVTR	O	O	0.69	7.11	106.18	28501	b2b7b9y3y4y5y6y8y9y10y12y17	13.77
P32119	Peroxiredoxin-2	ATAVVDGAFK	O	O	2.33	6.58	48.30	9116	y4y5y6y8	10.12
P32119	Peroxiredoxin-2	TDEGIAYR	N/A	O	N/A	N/A	N/A	N/A	N/A	N/A
P32119	Peroxiredoxin-2	EGGLGPLNIPLLADVTR	O	O	-1.80	6.89	98.02	28955	b2b5b6b8b10y3y4y5y7y8y18	14.38
P01033	Metalloproteinase inhibitor 1	LQSGTHCLWTDQLLQGSEK	O	O	-0.48	6.69	73.89	12801	b2y3y4y5y6y7y9y10y19	16.03
P01033	Metalloproteinase inhibitor 1	TYTVGCEECTVFPCLSIPCK	N/A	O	N/A	N/A	N/A	N/A	N/A	N/A
P01033	Metalloproteinase inhibitor 1	GFQALGDAADIR	O	O	0.92	7.49	65.00	16445	b2b4b5y2y4y5y7y8y9y12	8.54
P01033	Metalloproteinase inhibitor 1	EPGLCTWQSLR	O	O	0.66	6.28	68.38	12451	y3y4y6y7y11	13.48
P02790	Hemopexin	NFPSPVDAAFR	O	O	-0.93	9.37	72.79	6085217	b1b2b3b5b6b8b9b10by1y2y3y4y5y6y7y8y9y10y11	10.27
P02790	Hemopexin	GGYTLVSGYPK	O	O	-2.11	9.63	59.45	3772784	b3b4b5b6b7b8b9b10b11y2y3y4y5y6y7y8y9y11	4.29
P02790	Hemopexin	LLQDEFPGIPSPLDAAVECHR	O	O	0.38	9.84	89.83	9771462	b2b3b4b5b6b8b9b10b15b21y3y4y5y6y7y8y10y11y12y13y14y15y16y18y19y21	5.92
P02790	Hemopexin	YYCFQGNQFLR	O	O	-1.15	9.64	73.08	5058246	b1b2b3b4b5b6b7b8b9b10b11y1y2y3y4y5y6y7y8y9y10y11	5.20

Table 4. Target peptides list for LC-MRM method development extracted from discovery proteomics result. Continued

Uniprot accession number	Protein name	Peptide sequence	Peptides identified in discovery experiments	Peptides present in human SRM or PeptideAtlas DB	Precursor mass error (ppm)	Score	Retention Time (min)	Intensity	Matched MS/MS ion list	MS/MS ion RMS Mass Error (ppm)
P08571	CD 14	AFPALTSLDLSDNPGLGER	O	O	1.41	8.69	89.91	81741	b3b4b5b8b9b10b12b13b14b15b16b18b19y3y4y5y6y7 y9y10y11y12y13y14y15y17y19	15.54
P08571	CD 14	LTVGAAQVPAQLLVGALR	O	O	0.46	8.12	97.67	70026	b6b8b11b13b14b18y2y4y5y6y8y10y11y12y13y18	12.41
P08571	CD 14	VLSIAQAHSPAFSCEQVR	O	O	0.72	8.04	63.62	64849	b2b3b11b18y5y6y7y8y9y10y11y12y14y15y16y17y18	8.74
P13796	Plastin-2	VYALPEDLVEVNPK	O	O	0.23	6.73	80.60	31536	b2b11y5y8y10y11y12	13.48
P13796	Plastin-2	VNDDIIVNWVNETLR	O	O	1.85	6.58	107.16	24675	b2b4b12b13b15y1y3y5y6y7y8y10y15	21.38
P13796	Plastin-2	FSLVGIGGQDLNEGNR	O	O	-1.34	6.34	76.66	22496	b2b3b10b13b16y3y5y7y10y12y14y16	18.65
Q06141	Regenerating islet-derived protein 3-alpha	NPSTISSPGHCASLSR	O	O	-0.44	7.26	40.74	33452	b6y1y2y4y5y6y7y8y9y11y13y14y16	16.26
Q06141	Regenerating islet-derived protein 3-alpha	SWTDADLACQK	O	O	0.58	6.99	53.03	19345	b11y3y4y7y8y9y11	15.77

Table 5. Relative quantification of 20 target peptides by MRM MS (n = 10)

Uniprot accession	Protein name	Peptide sequence	1[a]	2	3	4	5	6	7	8	9	10	*p* - value
P05109	S100A8	ALNSIIDVYHK	0.0042[b]	0.0103	0.0183	0.0034	0.0068	0.0180	0.0128	0.0370	0.0499	0.0018	0.3095
P05109	S100A8	LLETECPQYIR	0.0079	0.0504	0.0316	0.0407	0.0414	0.0350	0.0219	0.0506	0.1054	0.0254	0.8413
P61769	Beta-2--microglobulin	VEHSDLSFSK	0.1268	0.1313	0.1561	0.6892	0.1687	0.7434	0.5189	0.2809	0.2890	0.8151	0.0556
P61769	Beta-2--microglobulin	VNHVTLSQPK	0.1964	0.2992	0.4258	1.5643	0.4829	2.0860	1.2799	0.3959	0.6402	1.8939	0.1508
P61769	leucine-rich alpha-2-glycoprotein	TLDLGENQLETLPPDLLR	0.3170	0.3762	0.2675	0.8344	0.4008	0.8121	0.5359	0.8267	0.6790	1.5606	0.0952
P02750	leucine-rich alpha-2-glycoprotein	ENQLEVLEVSWLHGLK	0.5040	0.7534	0.3785	1.6653	0.8808	1.3504	1.0078	1.8301	1.2210	3.0698	0.0556
Q12805	EGF-containing fibulin-like extracellular matrix protein 1	DIDECDIVPDACK	0.0144	0.0240	0.0164	0.0531	0.0172	0.0425	0.0460	0.0285	0.0356	0.0430	0.1508
Q12805	EGF-containing fibulin-like extracellular matrix protein 1	LNCEDIDECR	0.0053	0.0094	0.0057	0.0149	0.0067	0.0137	0.0169	0.0107	0.0121	0.0136	0.0952
P32119	peroxiredoxin-2	ATAVVDGAFK	0.0377	0.1358	0.0356	0.0996	0.0270	0.4200	0.0531	0.0692	0.1311	0.1770	0.1508
P32119	peroxiredoxin-2	TDEGIAYR	0.0713	0.2680	0.0643	0.2221	0.0979	0.9078	0.0979	0.1432	0.2825	0.3447	0.0952
P01033	metalloproteinase inhibitor 1	GFQALGDAADIR	0.0493	0.0789	0.0897	0.4399	0.0581	0.2638	0.2365	0.1629	0.1368	0.2876	0.1508
P01033	metalloproteinase inhibitor 1	EPGLCTWQSLR	0.0267	0.0565	0.0484	0.2968	0.0494	0.1976	0.1315	0.1111	0.1020	0.2142	0.1508
P02790	hemopexin	NFPSPVDAAFR	8.7288	12.6592	9.9991	5.1364	13.7726	8.6796	9.3705	10.4569	10.0714	12.0613	1.0000
P02790	hemopexin	YYCFQGNQFLR	3.9193	5.8562	4.6691	2.3558	6.3089	4.6674	4.4990	4.9386	5.1560	5.9324	0.8413
P08571	CD 14	AFPALTSLDLSDNPGLGER	0.2597	0.4261	0.3953	0.6005	0.5418	1.1933	0.2341	0.3390	0.4759	0.8741	0.8413
P08571	CD 14	VLSIAQAHSPAFSCEQVR	0.1905	0.3348	0.2776	0.4278	0.5346	0.7593	0.1870	0.2852	0.3929	0.7909	0.6905
P13796	Plastin-2	VYALPEDLVEVNPK	0.0897	0.2236	0.2503	0.2187	0.1449	0.5287	0.3768	0.3939	0.7401	0.2087	0.0556
P13796	Plastin-2	FSLVGIGGQDLNEGNR	0.0131	0.0328	0.0235	0.0229	0.0177	0.0454	0.0391	0.0426	0.0686	0.0233	0.0317
Q06141	REG 3	NPSTISSPGHCASLSR	0.0127	0.0285	0.0257	2.2883	0.0690	1.5606	6.1624	0.1145	0.0660	0.6588	0.1508
Q06141	REG 3	SWTDADLACQK	0.0011	0.0021	0.0017	0.1193	0.0048	0.0998	0.2669	0.0080	0.0037	0.0391	0.1508

[a] 1 – 5: (patients without GVHD), 6 - 10: (patients with GVHD)

[b] Peak area ratio (PAR): Light peptide peak area to heavy peptide peak area

3.5. Establishment of multiplexed MRM method for absolute quantification using high purity heavy peptide

To establish the MRM method for absolute quantification, 14 high-purity (>90% on average) heavy isotope-labeled peptide standards (SpikeTides^{TM}, JPT Peptide Technologies) were purchased. Optimized parameters for 88 MRM transitions of the 14 peptides are shown in Table 6. Next, we constructed 14 response curves for absolute quantification by spiking high-purity heavy peptides into the plasma matrix just before trypsin digestion (method described in section 2.11). The concentration range of each peptide for the response curve is shown in Table 7. Response curves for 14 peptides are illustrated in Figure 2 and other characteristics including slope, intercept, and R^2 (explained variance) are presented in Table 8. Fourteen response curves showed good linear correlations with R^2 values above 0.989. The LOD, LOQ, functional sensitivity (LLOQ), ULOQ, and CV of the lowest calibration point for all of 14 peptides are presented in Table 9. The median CV for all response curve data was 4.78% and CV at the functional sensitivity (LLOQ) point ranged from 1.65 to 15.90%. The lowest functional sensitivity of all peptides was 0.016 μg/mL, while the highest ULOQ was 257.438 μg/mL, revealing a dynamic range of protein abundance in the plasma. Finally, the best transition (quantifier) showing the lowest functional sensitivity, good linearity, and no interference was selected for absolute quantification in the verification patient cohort (Table 10).

Table 6. Optimized parameters of MRM transitions

Uniprot accession number	Protein_ name	Peptide sequence	Peptide category	Precursor Ion	Precursor ion charge	Product Ion	Product ion charge	Collision Energy	Retention Time (min)	Ion Name
sp|P61769|	Beta-2—macroglobulin	VEHSDLSFSK	Light	383.52	3	468.25	1	9	17.31	y4
sp|P61769|	Beta-2—macroglobulin	VEHSDLSFSK	Light	383.52	3	525.25	2	9	17.31	y9
sp|P61769|	Beta-2—macroglobulin	VEHSDLSFSK	Light	383.52	3	568.24	1	9	17.31	b5
sp|P61769|	Beta-2—macroglobulin	VEHSDLSFSK	Heavy	386.20	3	476.26	1	9	17.31	y4
sp|P61769|	Beta-2—macroglobulin	VEHSDLSFSK	Heavy	386.20	3	529.26	2	9	17.31	y9
sp|P61769|	Beta-2—macroglobulin	VEHSDLSFSK	Heavy	386.20	3	568.24	1	9	17.31	b5
sp|P61769|	Beta-2—macroglobulin	VNHVTLSQPK	Light	374.88	3	572.34	1	8.7	15.46	y5
sp|P61769|	Beta-2—macroglobulin	VNHVTLSQPK	Light	374.88	3	459.26	1	8.7	15.46	y4
sp|P61769|	Beta-2—macroglobulin	VNHVTLSQPK	Light	374.88	3	512.28	2	8.7	15.46	y9
sp|P61769|	Beta-2—macroglobulin	VNHVTLSQPK	Heavy	377.55	3	580.35	1	8.7	15.46	y5
sp|P61769|	Beta-2—macroglobulin	VNHVTLSQPK	Heavy	377.55	3	467.27	1	8.7	15.46	y4
sp|P61769|	Beta-2—macroglobulin	VNHVTLSQPK	Heavy	377.55	3	516.29	2	8.7	15.46	y9
sp|P02750|	Leucine-rich alpha-2-glycoprotein	ENQLEVLEVSWLHGLK	Light	632.01	3	761.94	2	18	37.93	y13
sp|P02750|	Leucine-rich alpha-2-glycoprotein	ENQLEVLEVSWLHGLK	Light	632.01	3	705.39	2	18	37.93	y12
sp|P02750|	Leucine-rich alpha-2-glycoprotein	ENQLEVLEVSWLHGLK	Light	632.01	3	640.87	2	18	37.93	y11
sp|P02750|	Leucine-rich alpha-2-glycoprotein	ENQLEVLEVSWLHGLK	Heavy	634.68	3	765.94	2	18	37.93	y13
sp|P02750|	Leucine-rich alpha-2-glycoprotein	ENQLEVLEVSWLHGLK	Heavy	634.68	3	709.40	2	18	37.93	y12
sp|P02750|	Leucine-rich alpha-2-glycoprotein	ENQLEVLEVSWLHGLK	Heavy	634.68	3	644.88	2	18	37.93	y11
sp|P02750|	Leucine-rich alpha-2-glycoprotein	TLDLGENQLETLPPDLLR	Light	679.70	3	924.55	1	19.7	35.32	y8
sp|P02750|	Leucine-rich alpha-2-glycoprotein	TLDLGENQLETLPPDLLR	Light	679.70	3	710.42	1	19.7	35.32	y6
sp|P02750|	Leucine-rich alpha-2-glycoprotein	TLDLGENQLETLPPDLLR	Light	679.70	3	613.37	1	19.7	35.32	y5
sp|P02750|	Leucine-rich alpha-2-glycoprotein	TLDLGENQLETLPPDLLR	Heavy	683.04	3	934.56	1	19.7	35.32	y8
sp|P02750|	Leucine-rich alpha-2-glycoprotein	TLDLGENQLETLPPDLLR	Heavy	683.04	3	720.43	1	19.7	35.32	y6
sp|P02750|	Leucine-rich alpha-2-glycoprotein	TLDLGENQLETLPPDLLR	Heavy	683.04	3	623.38	1	19.7	35.32	y5
sp|Q12805|	EGF-containing fibulin-like extracellular matrix protein 1	DIDECDIVPDACK	Light	775.33	2	1077.47	1	25	24.35	y9
sp|Q12805|	EGF-containing fibulin-like extracellular matrix protein 1	DIDECDIVPDACK	Light	775.33	2	590.26	1	25	24.35	y5
sp|Q12805|	EGF-containing fibulin-like extracellular matrix protein 1	DIDECDIVPDACK	Light	775.33	2	960.40	1	25	24.35	b8
sp|Q12805|	EGF-containing fibulin-like extracellular matrix protein 1	DIDECDIVPDACK	Heavy	779.34	2	1085.48	1	25	24.35	y9
sp|Q12805|	EGF-containing fibulin-like extracellular matrix protein 1	DIDECDIVPDACK	Heavy	779.34	2	598.27	1	25	24.35	y5
sp|Q12805|	EGF-containing fibulin-like extracellular matrix protein 1	DIDECDIVPDACK	Heavy	779.34	2	960.40	1	25	24.35	b8

Table 6. Optimized parameters of MRM transitions. Continued

Uniprot accession number	Protein_ name	Peptide sequence	Light Heavy	Precursor Ion	Precursor ion charge	Product Ion	Product ion charge	Collision Energy	Retention Time (min)	Ion Name
sp|Q12805|	EGF-containing fibulin-like extracellular matrix protein 1	LNCEDIDECR	Light	662.27	2	1096.40	1	21.5	18.14	y8
sp|Q12805|	EGF-containing fibulin-like extracellular matrix protein 1	LNCEDIDECR	Light	662.27	2	936.37	1	21.5	18.14	y7
sp|Q12805|	EGF-containing fibulin-like extracellular matrix protein 1	LNCEDIDECR	Light	662.27	2	807.33	1	21.5	18.14	y6
sp|Q12805|	EGF-containing fibulin-like extracellular matrix protein 1	LNCEDIDECR	Heavy	667.27	2	1106.41	1	21.5	18.14	y8
sp|Q12805|	EGF-containing fibulin-like extracellular matrix protein 1	LNCEDIDECR	Heavy	667.27	2	946.38	1	21.5	18.14	y7
sp|Q12805|	EGF-containing fibulin-like extracellular matrix protein 1	LNCEDIDECR	Heavy	667.27	2	817.34	1	21.5	18.14	y6
sp|P32119|	Peroxiredoxin-2	ATAVVDGAFK	Light	489.77	2	806.44	1	16.2	20.14	y8
sp|P32119|	Peroxiredoxin-2	ATAVVDGAFK	Light	489.77	2	735.40	1	16.2	20.14	y7
sp|P32119|	Peroxiredoxin-2	ATAVVDGAFK	Light	489.77	2	636.34	1	16.2	20.14	y6
sp|P32119|	Peroxiredoxin-2	ATAVVDGAFK	Heavy	493.77	2	814.45	1	16.2	20.14	y8
sp|P32119|	Peroxiredoxin-2	ATAVVDGAFK	Heavy	493.77	2	743.42	1	16.2	20.14	y7
sp|P32119|	Peroxiredoxin-2	ATAVVDGAFK	Heavy	493.77	2	644.35	1	16.2	20.14	y6
sp|P32119|	Peroxiredoxin-2	TDEGIAYR	Light	462.72	2	708.37	1	15.3	16.32	y6
sp|P32119|	Peroxiredoxin-2	TDEGIAYR	Light	462.72	2	579.32	1	15.3	16.32	y5
sp|P32119|	Peroxiredoxin-2	TDEGIAYR	Light	462.72	2	522.30	1	15.3	16.32	y4
sp|P32119|	Peroxiredoxin-2	TDEGIAYR	Heavy	467.73	2	718.38	1	15.3	16.32	y6
sp|P32119|	Peroxiredoxin-2	TDEGIAYR	Heavy	467.73	2	589.33	1	15.3	16.32	y5
sp|P32119|	Peroxiredoxin-2	TDEGIAYR	Heavy	467.73	2	532.31	1	15.3	16.32	y4
sp|P01033|	Metalloproteinase inhibitor 1	GFQALGDAADIR	Light	617.31	2	901.47	1	20.1	26.16	y9
sp|P01033|	Metalloproteinase inhibitor 1	GFQALGDAADIR	Light	617.31	2	830.44	1	20.1	26.16	y8
sp|P01033|	Metalloproteinase inhibitor 1	GFQALGDAADIR	Light	617.31	2	717.35	1	20.1	26.16	y7
sp|P01033|	Metalloproteinase inhibitor 1	GFQALGDAADIR	Heavy	622.32	2	911.48	1	20.1	26.16	y9
sp|P01033|	Metalloproteinase inhibitor 1	GFQALGDAADIR	Heavy	622.32	2	840.44	1	20.1	26.16	y8
sp|P01033|	Metalloproteinase inhibitor 1	GFQALGDAADIR	Heavy	622.32	2	727.36	1	20.1	26.16	y7
sp|P01033|	Metalloproteinase inhibitor 1	EPGLCTWQSLR	Light	673.83	2	950.45	1	21.9	27.12	y7
sp|P01033|	Metalloproteinase inhibitor 1	EPGLCTWQSLR	Light	673.83	2	790.42	1	21.9	27.12	y6
sp|P01033|	Metalloproteinase inhibitor 1	EPGLCTWQSLR	Light	673.83	2	689.37	1	21.9	27.12	y5
sp|P01033|	Metalloproteinase inhibitor 1	EPGLCTWQSLR	Heavy	678.83	2	960.46	1	21.9	27.12	y7
sp|P01033|	Metalloproteinase inhibitor 1	EPGLCTWQSLR	Heavy	678.83	2	800.43	1	21.9	27.12	y6
sp|P01033|	Metalloproteinase inhibitor 1	EPGLCTWQSLR	Heavy	678.83	2	699.38	1	21.9	27.12	y5

Table 6. Optimized parameters of MRM transitions. Continued

Uniprot accession number	Protein_ name	Peptide sequence	Light Heavy	Precursor Ion	Precursor ion charge	Product Ion	Product ion charge	Collision Energy	Retention Time (min)	Ion Name
sp|P13796|	Plastin-2	FSLVGIGGQDLNEGNR	Light	838.42	2	1229.59	1	27	29.62	y12
sp|P13796|	Plastin-2	FSLVGIGGQDLNEGNR	Light	838.42	2	1059.48	1	27	29.62	y10
sp|P13796|	Plastin-2	FSLVGIGGQDLNEGNR	Light	838.42	2	1002.46	1	27	29.62	y9
sp|P13796|	Plastin-2	FSLVGIGGQDLNEGNR	Heavy	843.43	2	1239.60	1	27	29.62	y12
sp|P13796|	Plastin-2	FSLVGIGGQDLNEGNR	Heavy	843.43	2	1069.49	1	27	29.62	y10
sp|P13796|	Plastin-2	FSLVGIGGQDLNEGNR	Heavy	843.43	2	1012.47	1	27	29.62	y9
sp|P13796|	Plastin-2	VYALPEDLVEVNPK	Light	793.43	2	1323.72	1	25.6	30.82	y12
sp|P13796|	Plastin-2	VYALPEDLVEVNPK	Light	793.43	2	1139.59	1	25.6	30.82	y10
sp|P13796|	Plastin-2	VYALPEDLVEVNPK	Light	793.43	2	570.30	2	25.6	30.82	y10
sp|P13796|	Plastin-2	VYALPEDLVEVNPK	Light	793.43	2	447.26	1	25.6	30.82	b4
sp|P13796|	Plastin-2	VYALPEDLVEVNPK	Heavy	797.43	2	1331.73	1	25.6	30.82	y12
sp|P13796|	Plastin-2	VYALPEDLVEVNPK	Heavy	797.43	2	1147.61	1	25.6	30.82	y10
sp|P13796|	Plastin-2	VYALPEDLVEVNPK	Heavy	797.43	2	574.31	2	25.6	30.82	y10
sp|P13796|	Plastin-2	VYALPEDLVEVNPK	Heavy	797.43	2	447.26	1	25.6	30.82	b4
sp|Q06141|	Regenerating islet-derived protein 3-alpha	SWTDADLACQK	Light	647.79	2	1021.46	1	21.1	21.96	y9
sp|Q06141|	Regenerating islet-derived protein 3-alpha	SWTDADLACQK	Light	647.79	2	920.41	1	21.1	21.96	y8
sp|Q06141|	Regenerating islet-derived protein 3-alpha	SWTDADLACQK	Light	647.79	2	734.35	1	21.1	21.96	y6
sp|Q06141|	Regenerating islet-derived protein 3-alpha	SWTDADLACQK	Heavy	651.80	2	1029.48	1	21.1	21.96	y9
sp|Q06141|	Regenerating islet-derived protein 3-alpha	SWTDADLACQK	Heavy	651.80	2	928.43	1	21.1	21.96	y8
sp|Q06141|	Regenerating islet-derived protein 3-alpha	SWTDADLACQK	Heavy	651.80	2	742.36	1	21.1	21.96	y6
sp|Q06141|	Regenerating islet-derived protein 3-alpha	NPSTISSPGHCASLSR	Light	557.60	3	686.84	2	15.3	17.34	y13
sp|Q06141|	Regenerating islet-derived protein 3-alpha	NPSTISSPGHCASLSR	Light	557.60	3	636.31	2	15.3	17.34	y12
sp|Q06141|	Regenerating islet-derived protein 3-alpha	NPSTISSPGHCASLSR	Light	557.60	3	579.77	2	15.3	17.34	y11
sp|Q06141|	Regenerating islet-derived protein 3-alpha	NPSTISSPGHCASLSR	Light	557.60	3	492.74	2	15.3	17.34	y9
sp|Q06141|	Regenerating islet-derived protein 3-alpha	NPSTISSPGHCASLSR	Heavy	560.94	3	691.84	2	15.3	17.34	y13
sp|Q06141|	Regenerating islet-derived protein 3-alpha	NPSTISSPGHCASLSR	Heavy	560.94	3	641.32	2	15.3	17.34	y12
sp|Q06141|	Regenerating islet-derived protein 3-alpha	NPSTISSPGHCASLSR	Heavy	560.94	3	584.77	2	15.3	17.34	y11
sp|Q06141|	Regenerating islet-derived protein 3-alpha	NPSTISSPGHCASLSR	Heavy	560.94	3	497.74	2	15.3	17.34	y9

Table 7. Concentration range of each peptide used for response curve establishment

Uniprot accession number	Protein name	Peptide	Response curve calibration point							
			1 (highest) ug/ml	2	3	4	5	6	7	8 (lowest) ug/ml
P61769	Beta-2—microglobulin	VEHSDLSFSK	8.792	4.396	2.198	1.099	0.550	0.275	0.137	0.069
P61769	Beta-2—microglobulin	VNHVTLSQPK	8.792	4.396	2.198	1.099	0.550	0.275	0.137	0.069
Q12805	EGF-containing fibulin-like extracellular matrix protein 1	DIDECDIVPDACK	3.296	1.648	0.824	0.412	0.206	0.103	0.051	0.026
Q12805	EGF-containing fibulin-like extracellular matrix protein 1	LNCEDIDECR	6.591	3.296	1.648	0.824	0.412	0.206	0.103	0.051
P32119	Peroxiredoxin-2	ATAVVDGAFK	5.437	2.718	1.359	0.680	0.340	0.170	0.085	0.042
P32119	Peroxiredoxin-2	TDEGIAYR	5.437	2.718	1.359	0.680	0.340	0.170	0.085	0.042
P01033	Metalloproteinase inhibitor 1	GFQALGDAADIR	10.348	5.174	2.587	1.293	0.647	0.323	0.162	0.081
P01033	Metalloproteinase inhibitor 1	EPGLCTWQSLR	10.348	5.174	2.587	1.293	0.647	0.323	0.162	0.081
P13796	Plastin-2	VYALPEDLVEVNPK	17.528	8.764	4.382	2.191	1.096	0.548	0.274	0.137
P13796	Plastin-2	FSLVGIGGQDLNEGNR	8.764	4.382	2.191	1.096	0.548	0.274	0.137	0.068
P02750	Leucine-rich alpha-2-glycoprotein	TLDLGENQLETLPPDLLR	171.625	85.813	42.906	21.453	10.727	5.363	2.682	1.341
P02750	Leucine-rich alpha-2-glycoprotein	ENQLEVLEVSWLHGLK	257.438	128.719	64.359	32.180	16.090	8.045	N/A	N/A
Q06141	REG 3 alpha	SWTDADLACQK	2.069	1.035	0.517	0.259	0.129	0.065	0.032	0.016
Q06141	REG 3 alpha	NPSTISSPGHCASLSR	8.278	4.139	2.069	1.035	0.517	0.259	0.129	0.065

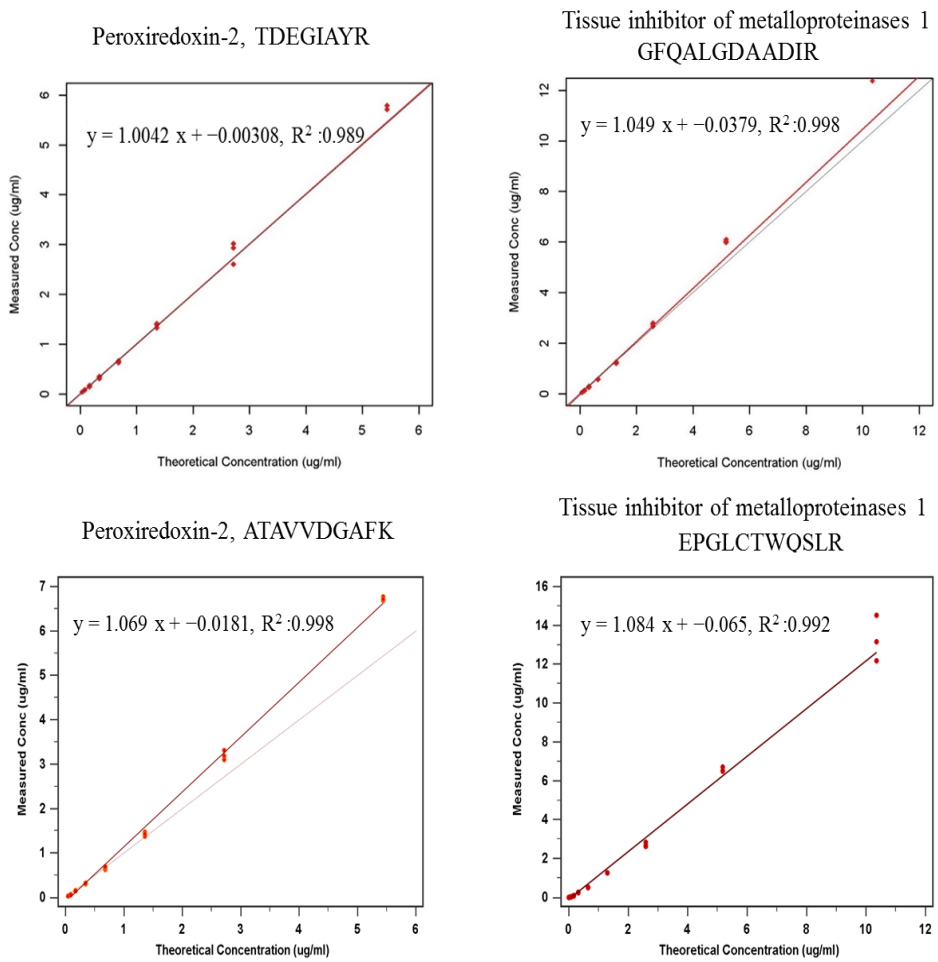

Figure 2. Response curves of 14 target peptides for MRM-MS based absolute quantification.

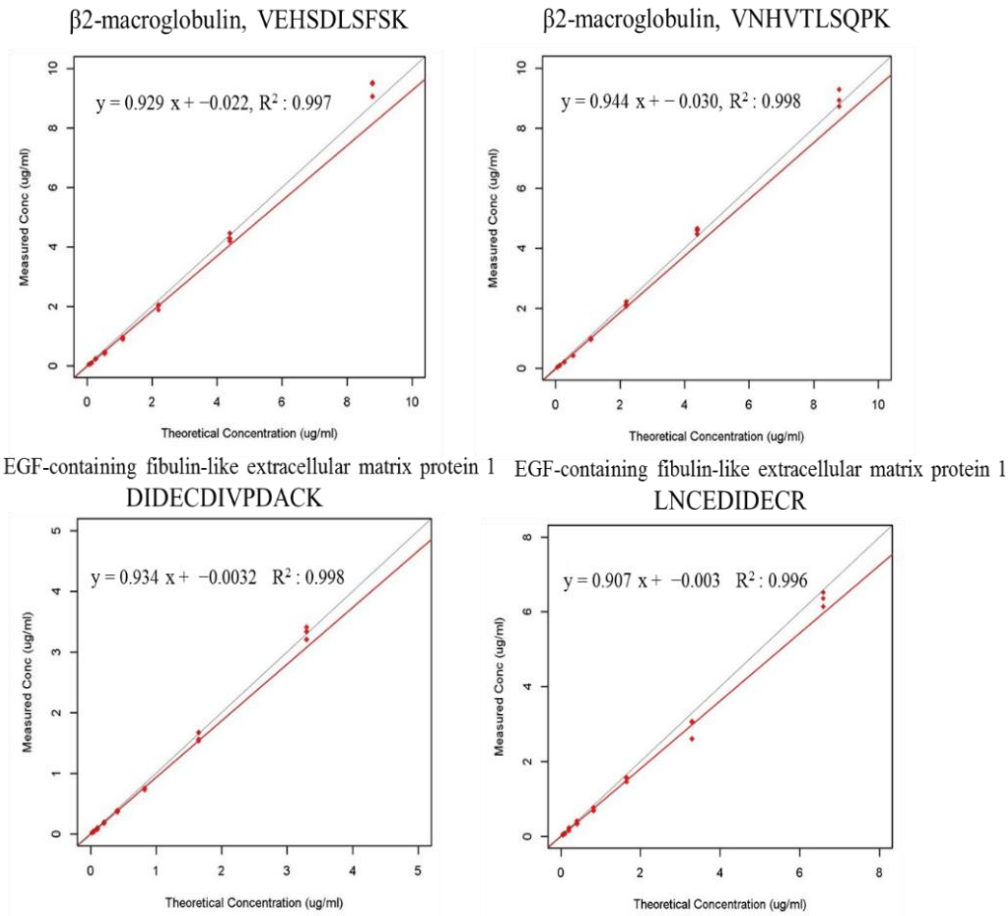

Figure 2. Response curves of 14 target peptides for MRM-MS based absolute quantification. Continued

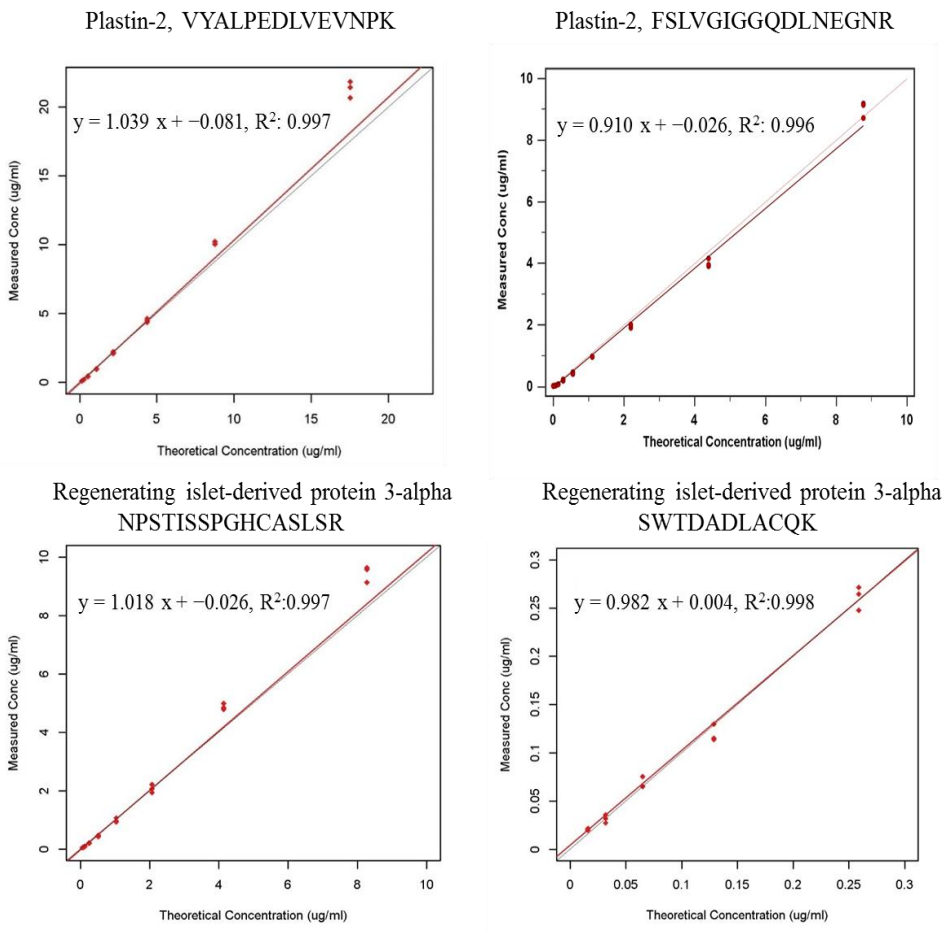

Figure 2. Response curves of 14 target peptides for MRM-MS based absolute quantification. Continued

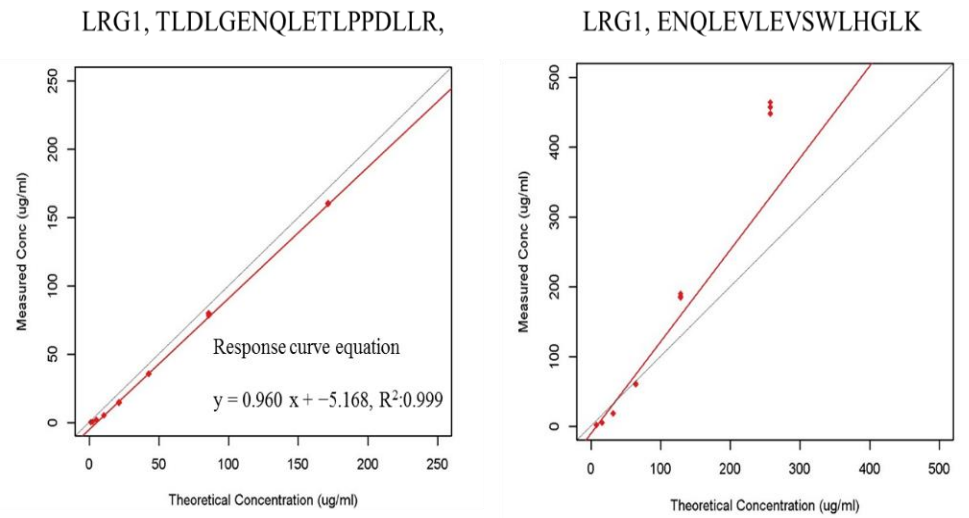

Figure 2. Response curves of 14 target peptides for MRM-MS based absolute quantification. Continued

Table 8. Characteristics of response curves for 14 peptides

Protein name	Peptide	Transition.id	Slope	y-intercept	Rsquare
Beta-2--microglobulin	VEHSDLSFSK	3.y4.1.0	0.929	-0.022	0.997
Beta-2--microglobulin	VNHVTLSQPK	3.y9.2.0	0.944	-0.030	0.999
EGF-containing fibulin-like extracellular matrix protein 1	DIDECDIVPDACK	2.y5.1.0	0.935	-0.003	0.998
EGF-containing fibulin-like extracellular matrix protein 1	LNCEDIDECR	2.y8.1.0	0.907	-0.003	0.996
Peroxiredoxin-2	ATAVVDGAFK	2.y8.1.0	1.069	-0.018	0.998
Peroxiredoxin-2	TDEGIAYR	2.y5.1.0	1.004	-0.003	0.989
Metalloproteinase inhibitor 1	GFQALGDAADIR	2.y7.1.0	1.050	-0.038	0.998
Metalloproteinase inhibitor 1	EPGLCTWQSLR	2.y6.1.0	1.085	-0.066	0.992
Plastin-2	VYALPEDLVEVNPK	2.y10.1.0	1.039	-0.082	0.998
Plastin-2	FSLVGIGGQDLNEGNR	2.y12.1.0	0.911	-0.026	0.996
Leucine-rich α-2-glycoprotein	TLDLGENQLETLPPDLLR	3.y6.1.0	0.961	-5.175	0.999
Leucine-rich α-2-glycoprotein	ENQLEVLEVSWLHGLK	3.y12.2.0	1.317	-10.934	0.989
REG 3 alpha	NPSTISSPGHCASLSR	3.y11.2.0	1.018	-0.026	0.998
REG 3 alpha	SWTDADLACQK	2.y9.1.0	0.983	0.004	0.998

Table 9. Response curve analysis result

Protein name	Uniprot KB accession number	Peptide sequence	Precursor ion charge	Product Ion type	Product ion charge	CV (%) at LLOQ	LOD (ug/ml)	LOQ (ug/ml)	Functional sensitivity (LLOQ) (ug/ml)	ULOQ (ug/ml)
Beta-2—macroglobulin	P61769	VEHSDLSFSK	3	y4	1	5.40	0.0026	0.00876	0.069	8.790
Beta-2—macroglobulin	P61769	VNHVTLSQPK	3	y9	2	4.81	0.0016	0.005	0.069	8.790
EGF-containing fibulin-like extracellular matrix protein 1	Q12805	DIDECDIVPDACK	2	y5	1	8.85	0.0122	0.041	0.026	3.290
EGF-containing fibulin-like extracellular matrix protein 1	Q12805	LNCEDIDECR	2	y8	1	9.74	0.0150	0.050	0.051	6.590
peroxiredoxin-2	P32119	ATAVVDGAFK	2	y8	1	6.77	0.0037	0.012	0.042	5.437
peroxiredoxin-2	P32119	TDEGIAYR	2	y5	1	2.62	0.0025	0.008	0.042	5.437
metalloproteinase inhibitor 1	P01033	GFQALGDAADIR	2	y7	1	1.65	0.0054	0.018	0.081	10.348
metalloproteinase inhibitor 1	P01033	EPGLCTWQSLR	2	y6	1	15.90	0.0140	0.047	0.081	10.348
Plastin-2	P13796	VYALPEDLVEVNPK	2	y10	1	6.27	0.0089	0.0297	0.137	17.528
Plastin-2	P13796	FSLVGIGGQDLNEGNR	2	y12	1	11.32	0.0210	0.0700	0.068	8.764
leucine-rich alpha-2-glycoprotein	P02750	TLDLGENQLETLPPDLLR	3	y6	1	3.63	0.0279	0.0930	1.340	171.620
leucine-rich alpha-2-glycoprotein	P02750	ENQLEVLEVSWLHGLK	3	y12	2	4.08	0.0335	0.1110	8.045	257.438
REG 3 alpha	Q06141	NPSTISSPGHCASLSR	3	y11	2	2.61	0.0052	0.017	0.065	8.278
REG 3 alpha	Q06141	SWTDADLACQK	2	y9	1	5.08	0.0054	0.0181	0.016	2.069

Table 10. Best MRM transition of 14 target peptides for absolute quantification

Uniprot accession number	Protein name	Peptide sequence	Product ion type	Precursor ion charge	Product ion charge	Peptide category	Precursor ion (m/z)	Product ion (m/z)	Collision energy (eV)	Retention time (min)
P61769	Beta 2 microglobulin	VEHSDLSFSK	y4	3	1	Light	383.52	468.25	9	17.31
		VEHSDLSFSK	y4	3	1	Heavy	386.20	476.26	9	17.31
P61769	Beta 2 microglobulin	VNHVTLSQPK	y9	3	2	Light	374.88	512.28	8.7	15.46
		VNHVTLSQPK	y9	3	2	Heavy	377.55	516.29	8.7	15.46
Q12805	EGF containing fibulin like extracellular matrix protein 1	DIDECDIVPDACK	y5	2	1	Light	775.33	590.26	25	24.35
		DIDECDIVPDACK	y5	2	1	Heavy	779.34	598.27	25	24.35
Q12805	EGF containing fibulin like extracellular matrix protein 1	LNCEDIDECR	y8	2	1	Light	662.27	1096.40	21.5	18.14
		LNCEDIDECR	y8	2	1	Heavy	667.27	1106.41	21.5	18.14
P32119	Peroxiredoxin 2	ATAVVDGAFK	y8	2	1	Light	489.77	806.44	16.2	20.14
		ATAVVDGAFK	y8	2	1	Heavy	493.77	814.45	16.2	20.14
P32119	Peroxiredoxin 2	TDEGIAYR	y5	2	1	Light	462.72	579.32	15.3	16.32
		TDEGIAYR	y5	2	1	Heavy	467.73	589.33	15.3	16.32
P01033	Metalloproteinase inhibitor 1	GFQALGDAADIR	y7	2	1	Light	617.31	717.35	20.1	26.16
		GFQALGDAADIR	y7	2	1	Heavy	622.32	727.36	20.1	26.16
P01033	Metalloproteinase inhibitor 1	EPGLCTWQSLR	y6	2	1	Light	673.83	790.42	21.9	27.12
		EPGLCTWQSLR	y6	2	1	Heavy	678.83	800.43	21.9	27.12
P13796	Plastin 2	VYALPEDLVEVNPK	y10	2	1	Light	793.43	1139.59	25.6	30.82
		VYALPEDLVEVNPK	y10	2	1	Heavy	797.43	1147.61	25.6	30.82
P13796	Plastin 2	FSLVGIGGQDLNEGNR	y12	2	1	Light	838.42	1229.59	27	29.62
		FSLVGIGGQDLNEGNR	y12	2	1	Heavy	843.43	1239.60	27	29.62
P02750	Leucine rich alpha 2 glycoprotein	TLDLGENQLETLPPDLLR	y6	3	1	Light	679.70	710.42	19.7	35.32
		TLDLGENQLETLPPDLLR	y6	3	1	Heavy	683.04	720.43	19.7	35.32
P02750	Leucine rich alpha 2 glycoprotein	ENQLEVLEVSWLHGLK	y12	3	2	Light	632.01	705.39	18	37.93
		ENQLEVLEVSWLHGLK	y12	3	2	Heavy	634.68	709.40	18	37.93
Q06141	REG 3 alpha	SWTDADLACQK	y9	2	1	Light	647.79	1021.46	21.1	21.96
		SWTDADLACQK	y9	2	1	Heavy	651.80	1029.48	21.1	21.96
Q06141	REG 3 alpha	NPSTISSPGHCASLSR	y11	3	2	Light	557.60	579.77	15.3	17.34
		NPSTISSPGHCASLSR	y11	3	2	Heavy	560.94	584.77	15.3	17.34

3.6. Absolute quantification of candidate biomarkers with multiplexed MRM methods

A multiplexed MRM method based on the capillary flow LC with triple quadrupole MS was developed to verify the biomarker candidates. This method uses 14 high-purity stable isotope-labeled peptides standards to quantify 7 biomarker candidate proteins in tryptic digests of plasma in 80 min. Using the multiplexed MRM method, we precisely determined the absolute concentrations of 14 candidate peptides in 89 plasma samples from patients. The correlation coefficient of the peak area ratio (light to heavy) between two technical LC-MS runs for each peptide, shown in Figure 3, and ranged from 0.972 to 0.999, demonstrating good reproducibility for technical LC-MS replicates. Two surrogate peptides of each protein differed in absolute abundance by 1.2–2-fold, which are not highly different values. This discrepancy in abundance may be because of inefficient trypsin digestion and unknown modifications of specific peptides [40]. Figure 4 shows the linear relationship of the log-transformed concentration of two different peptides from each corresponding protein, showing a good linear correlation coefficient (r = 0.928–0.996). This linear relationship data are beneficial for excluding surrogate peptides which cannot be used for quantification by examining correlation of multiple surrogate peptides per protein and can be used to identify an outliers caused by sample-specific signal interference or incomplete trypsin digestion.

.

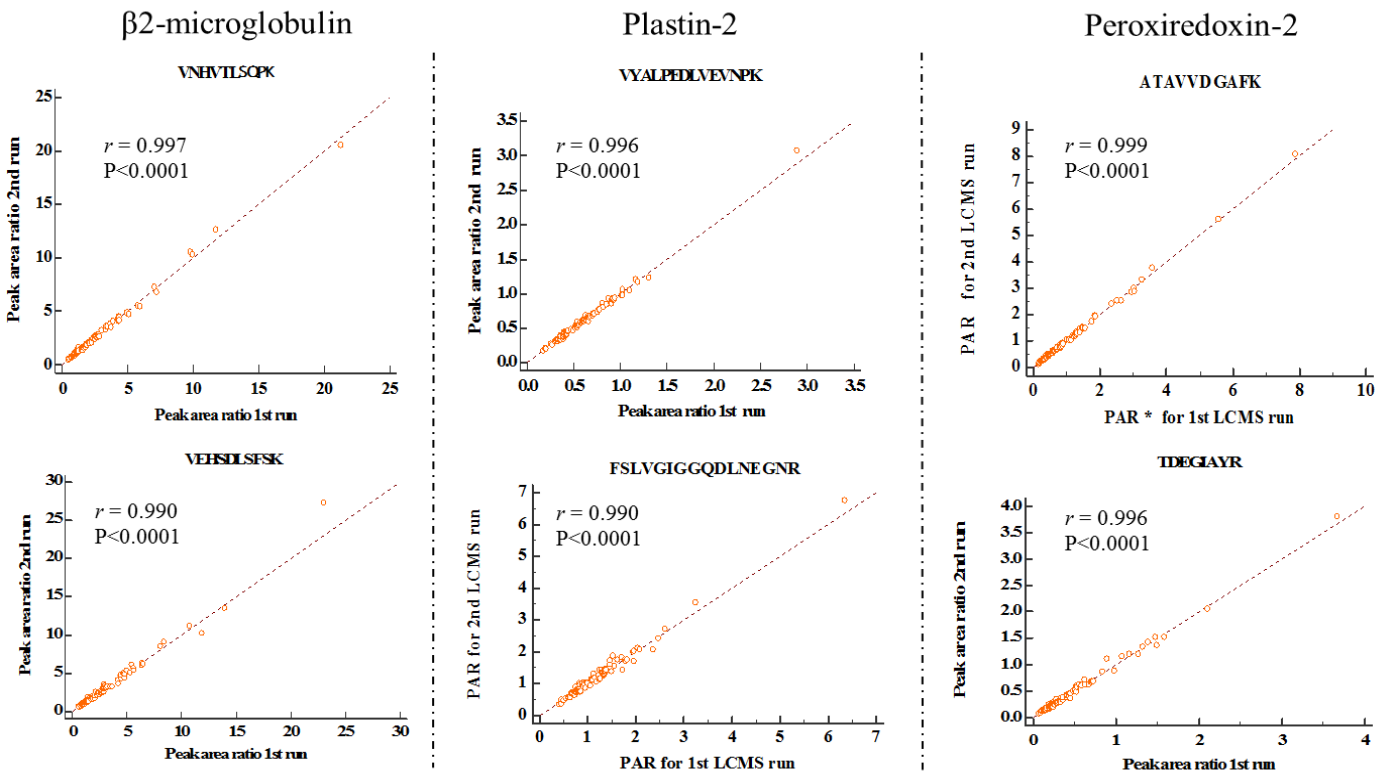

Figure 3. Correlation analysis of PAR for two technical LC-MS replicates run
*** Peak area ratio (Ratio of light peptide area to heavy peptide area)**

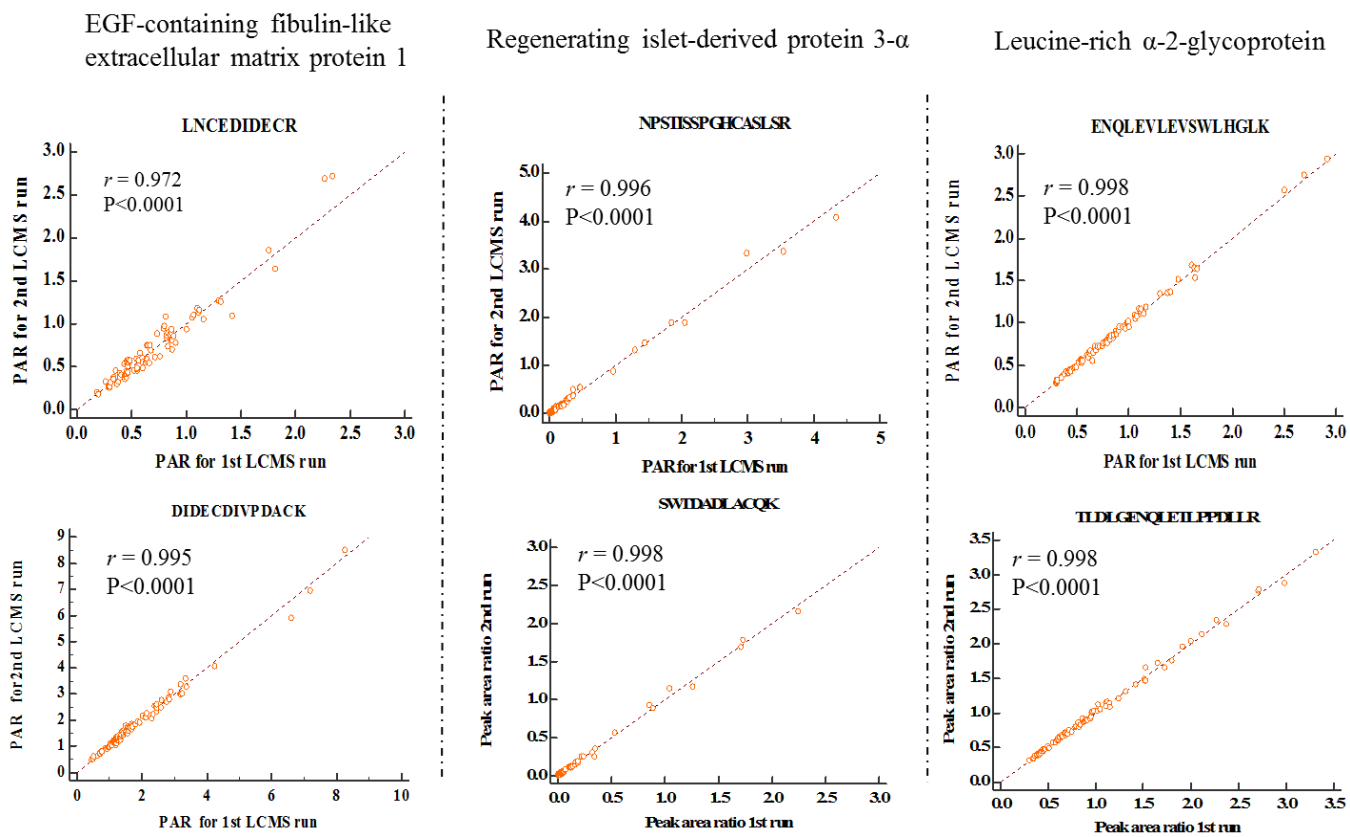

Figure 3. Correlation analysis of PAR (peak area ratio) for two technical LC-MS replicates run. Continued

Tissue inhibitor of metalloproteinases 1

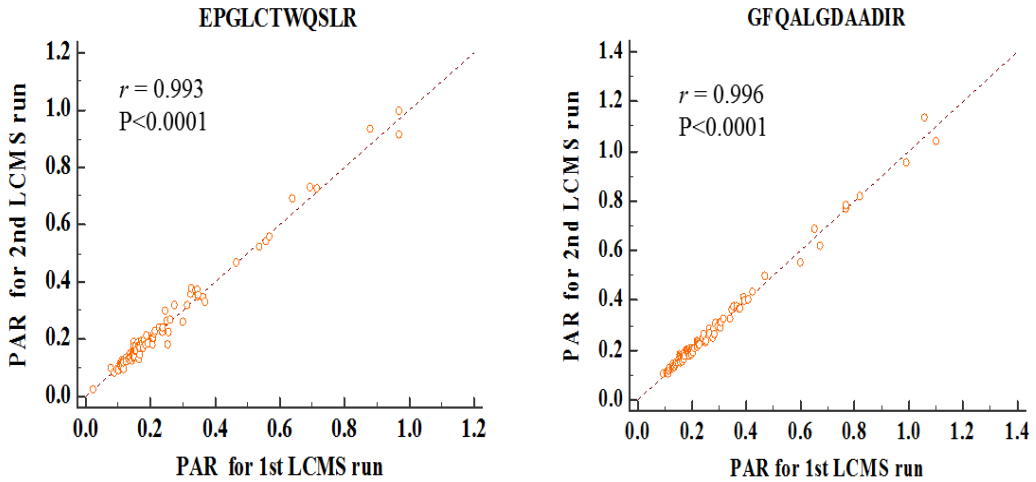

Figure 3. Correlation analysis of PAR (peak area ratio) for two technical LC-MS replicates run. Continued

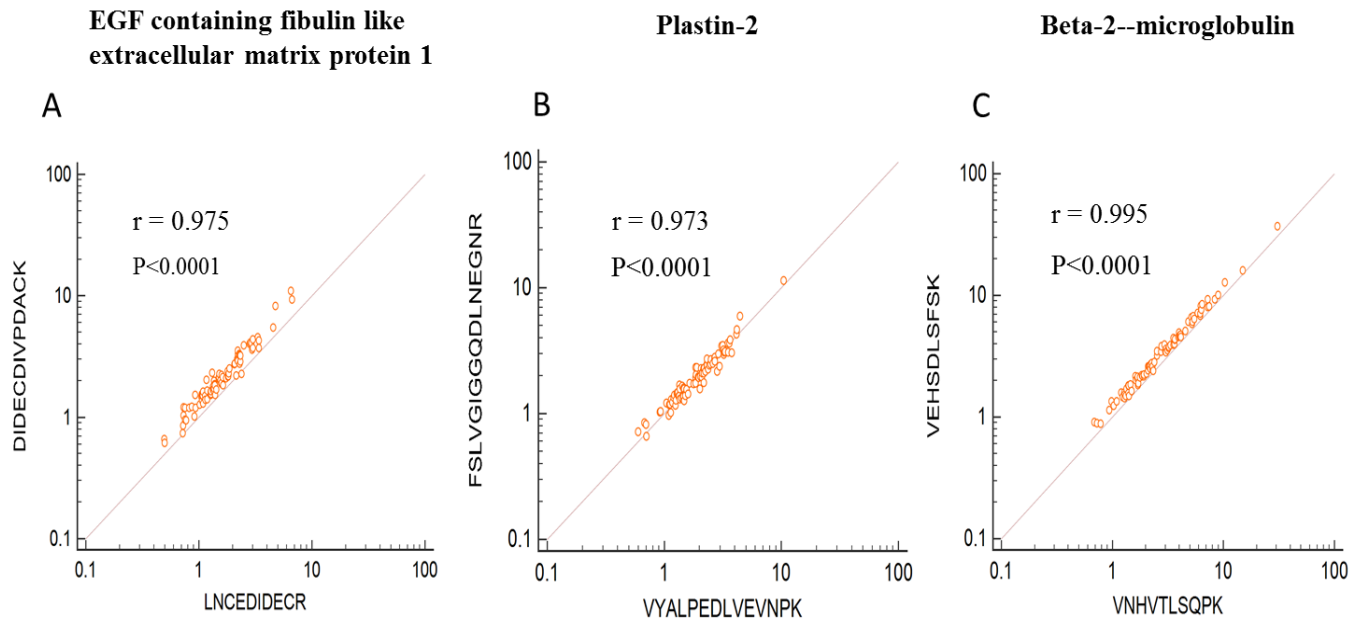

Figure 4. Linear relationship of two surrogate peptides for each protein. A: EGF containing fibulin like extracellul ar matrix protein 1, B: Plastin-2, C: Beta-2--microglobulin *r:* Pearson correlation coefficient
Dashed line: a line of equality (y=x) line in the graph. Base-10 log transformed concentration of each peptide (ug/mL) from 89 verification set are used for correlation analysis.

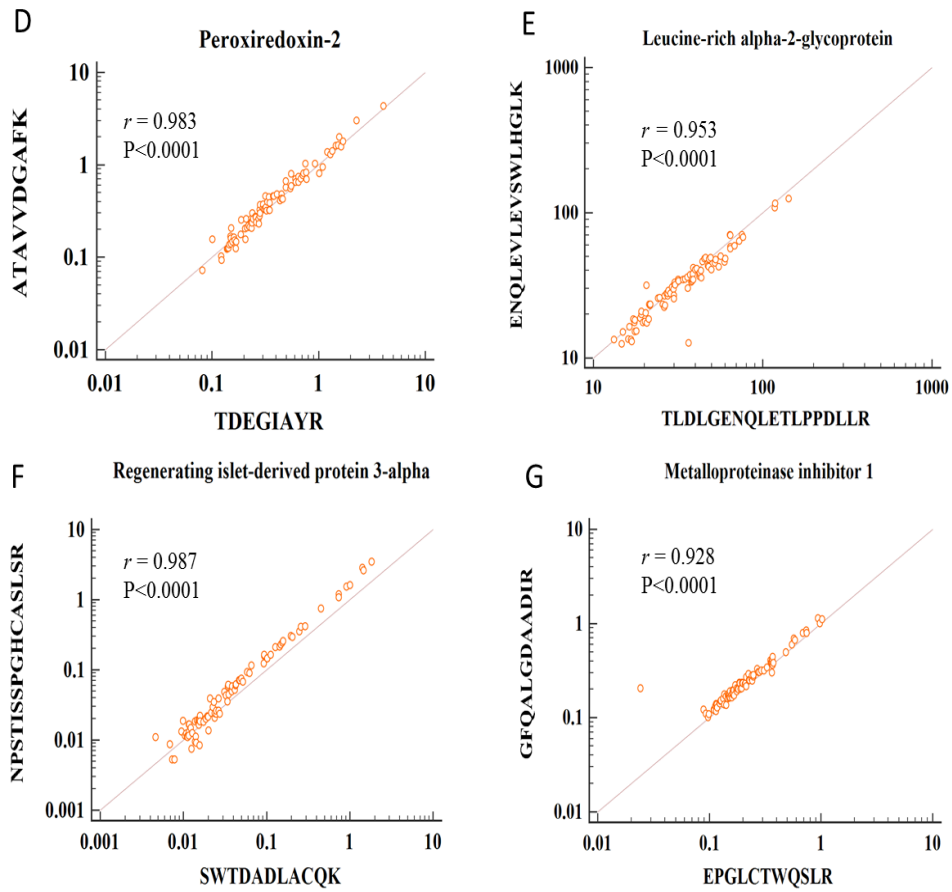

Figure 4. Linear relationship of two surrogate peptides for each protein: D: Peroxiredoxin-2, E: Leucine-rich α-2-glycoprotein, F: Regenerating islet-derived protein 3-α, G: Metalloproteinasesinhibitor 1. Continued

3.7 Predictive value of the post-engraftment biomarker level for the risk of aGVHD

In the entire verification set, 40 patients (44.9%) developed aGVHD: overall clinical grade I in 9 (10.1%), grade II in 14 (15.7%), grade III in 12 (13.5%), and grade IV in 5 (5.6%) of patients. Plasma samples were obtained a median of 16 (range, 12-29) days after alloHSCT and a median of four (range, 0-16) days from the engraftment day (Figure 5). Univariable analysis of clinical characteristics and the biomarker level to predict the risk of aGVHD indicated that only GVHD prophylaxis and the level of tissue inhibitor of metalloproteinase 1 (TIMP-1) were significantly associated with aGVHD risk (Table 11). Patients with high level of TIMP-1 were approximately twice as likely to experience aGVHD compared to patients with low level of TIMP-1. All other candidate biomarkers showed a trend toward increased risk of aGVHD in patients with high level as compared with the patients with low level, but these trends were not significant. After adjustment for the most important clinical characteristics, leucine-rich α-2-glycoprotein (LRG), fibrillin-like protein and TIMP-1 showed significant association with the risk of aGVHD (Table 12). Using a predefined two-step variable selection algorithm, we constructed an optimal multivariable Cox model containing two clinical characteristics and two biomarkers. In line with the univariable analysis results, the model indicated that patients with high TIMP-1 and plastin-2 level had 2.3 and 1.7 times as higher risk of aGVHD, respectively, as compared to the low-level counterparts independently of other covariates (Table 13). Among the 40 patients who developed aGVHD, there was no significant correlation between the biomarker level and the maximal grade of aGVHD (Figure 6).

3.8 Predictive value of the post-engraftment biomarker level for NRM

During a median follow-up of 7.1 years, 20 patients (22.5%) developed NRM. The univariable analysis showed that donor-recipient relationship, HLA match, donor age, GVHD prophylaxis, and the plasma level of β2-microglobulin, TIMP-1, and regenerating islet-derived protein 3-α (REG3α) are associated with NRM (Table 11). Among the biomarkers, TIMP-1 and REG3α were predictive of NRM even after adjustment for clinical characteristics (Table 14). As in the results from aGVHD risk analysis, all other biomarkers showed a trend of increased NRM in high-level patients versus low-level patients. The optimal multivariable model was found to contain five variables (two clinical predictors and three biomarkers), three of which were also included in the optimal model to predict aGVHD risk (Table 15). High plasma level of all three biomarkers included in the model was shown to confer NRM larger than twice that of the patients with low plasma level of the corresponding proteins, although only REG3α reached statistical significance.

3.9 Association of the biomarker panel score with the risk of aGVHD and NRM

Using biomarkers that were included at least one of the optimal Cox models to predict the risk of aGVHD and NRM, i.e. TIMP-1, plastin-2, and REG3α, we defined a new composite variable, the biomarker panel score, as the number of markers that are at high level in a given patient. Therefore, the biomarker panel score ranged from zero to three. Reducing the whole set of candidate biomarkers into a core subset was necessary because many of the candidate markers showed high pairwise correlation in the plasma level (Figure 7). Remarkably, the biomarker panel score showed significant association both with the risk of aGVHD and with NRM both before and after adjustment for the clinical characteristics in the Cox model (Table 16). In addition, the hazard ratio (HR)

for NRM was higher than that for the risk of aGVHD, suggesting the additional role of the biomarker panel score in predicting aGVHD-unrelated NRM.

Nested-model likelihood ratio test indicated a significant contribution of the biomarker panel score to the model performance when it was added to the model containing clinical characteristics only both to predict aGVHD risk and to predict NRM (LR-test $P = 0.023$ and < 0.001, respectively). Distribution of the 5-CVC generated using 200 independent random splitting of the dataset also indicated that discrimination capability of the model containing clinical characteristics plus biomarker panel score was significantly better than that of the model containing clinical characteristics only **(**Figure 8**).** The addition of the biomarker panel score correctly reclassified 29.6% of the patients who developed aGVHD within 6 months after alloHSCT and 8.8% of the patients who did not develop aGVHD within this timeframe; the NRI was 38.3%. However, this was not significant ($P = 0.074$; Table 17). On the other hand, the model containing clinical characteristics plus biomarker panel score correctly reclassified 32.7% of the patients who died without relapse within 1 year from alloHSCT and 21% of the patients who did not die without relapse within 1 year after alloHSCT as compared to the model containing clinical characteristics only. The reclassification amount was significant with NRI of 53.7% ($P = 0.032$; Table 18).

3.10 Cumulative incidence of aGVHD and NRM according to the biomarker level

As shown in the Figures 9 and 10, patients with high plasma level showed a consistent trend of higher cumulative incidence of aGVHD and cumulative NRM as compared with the patients with low plasma level for all candidate biomarkers. Among those, TIMP-1, plastin-2, and REG3α, which together comprised the biomarker panel score, were significantly correlated with cumulative NRM (Figure 10), whereas no single

biomarker level showed a significant correlation with the cumulative incidence of aGVHD. Likewise, patients with a higher biomarker panel score exhibited a significantly higher cumulative NRM than patients with a lower biomarker panel score (Figure 11). The difference in the cumulative incidence of aGVHD according to the biomarker panel score was not significant, although the overall trend indicated higher incidence in patients with a higher score. In accordance with these results, the Fine-Gray model also revealed significant subdistribution hazard ratios (HRs) for NRM of the biomarker panel score in both univariable analysis and multivariable analysis (Table 19).

Because the biomarker panel score showed significant correlation with the cause-specific hazard of aGVHD in the preceding Cox model analysis (HR [95% CI], 1.57 [1.13-2.18] and 1.55 [1.07-2.25] in the univariable analysis and multivariable analysis, respectively) but not significant correlation with the subdistribution hazard of aGVHD (HR [95% CI], 1.3 [0.98-1.71] and 1.2 [0.85-1.69] in the univariable analysis and multivariable analysis, respectively), we examined if this discrepancy was caused by the increased competing risk of aGVHD, i.e. death without aGVHD, in patients with a high biomarker panel score. Indeed, the subdistribution HR (95% CI) for death without aGVHD was 1.49 (0.87-2.53) in the univariable model and 1.61 (0.95-2.73) in the multivariable model, both of which were numerically higher than the subdistribution HRs for aGVHD. These data suggest that the significant cause-specific HR for aGVHD of the biomarker panel score did not translate into the significantly higher actual incidence of aGVHD in higher-score patients because the score was also associated with incidence of aGVHD-unrelated death, a competing event of aGVHD. Among the 21 patients who died without aGVHD, the most common cause of death was relapse (n = 10), followed by infection (n = 4) and multiple organ dysfunction syndrome (n =3).

3.11 Organ-specific association of the biomarker level and aGVHD risk

Plasma proteins may reflect target organ-specific injury and therefore can be used as diagnostic biomarkers for organ-specific aGVHD (42,43). By extension of this concept, I hypothesized that predictive biomarkers might also indicate organ-specific risk of future aGVHD occurrence. Thus, I separately compared the cumulative incidence of aGVHD involving each of the three major target organs, i.e., skin, gastrointestinal tract, or liver, between patients with high level and patients with low level of each of seven candidate biomarkers. The results showed that there is no significant organ-specific correlation of the biomarker level with the risk of aGVHD, although visual inspection of the cumulative incidence curves suggested a potential predictive value of LRG for skin aGVHD, REG3α for gastrointestinal aGVHD, and TIMP-1 for both skin aGVHD and liver aGVHD (Figure 12-14). Likewise, the biomarker panel score did not significantly correlate with the risk of organ-specific aGVHD, but the risk for skin aGVHD and liver aGVHD tended to be higher in patients with a higher biomarker panel score (Figure 15).

Table 11. Univariable Cox proportional hazards regression analysis for the risk of aGVHD and NRM in the verification set (n = 89)

Variable	Risk of aGVHD		NRM	
	HR (95% CI)	*P* value	HR (95% CI)	*P* value
Age at alloHSCT: ≥45 vs. <45	1.58 (0.85-2.96)	0.15	1.18 (0.49-2.86)	0.709
Sex: female vs. male	0.96 (0.51-1.8)	0.889	0.78 (0.31-1.97)	0.605
Diagnosis: malignant vs. benign	0.61 (0.31-1.21)	0.156	0.56 (0.22-1.41)	0.217
Stem cell source: PBSC vs. BM	0.84 (0.3-2.36)	0.737	0.44 (0.13-1.53)	0.198
Donor relationship: unrelated vs. related	1.57 (0.84-2.94)	0.155	3.83 (1.47-10)	0.006
HLA match: mismatched vs. matched	1.84 (0.96-3.54)	0.066	2.43 (1-5.88)	0.049
Donor sex: female vs. male	1.03 (0.52-2.02)	0.933	1.07 (0.41-2.78)	0.89
Donor age: ≥40 vs. <40	0.85 (0.45-1.6)	0.616	0.29 (0.1-0.88)	0.029
Conditioning: MAC[e]/RIC[f] vs. NMAC[g]	1 (0.52-1.92)	0.989	0.64 (0.27-1.56)	0.328
GVHD prophylaxis				
CNI[a] + MTX[b]/MMF[c] vs. CNI alone	0.21 (0.09-0.49)	<0.001	0.22 (0.08-0.67)	0.007
CNI + ATG[d] ± MTX vs. CNI alone	0.27 (0.12-0.61)	0.002	0.23 (0.08-0.65)	0.006
Biomarkers: high vs. low				
β2-microglobulin	1.49 (0.8-2.78)	0.213	2.79 (1.07-7.26)	0.036
LRG	1.78 (0.94-3.37)	0.075	1.37 (0.57-3.32)	0.482
Fibrillin-like protein	1.62 (0.87-3.05)	0.131	1.38 (0.57-3.34)	0.472
Peroxiredoxin-2	1.4 (0.75-2.6)	0.295	1.54 (0.63-3.78)	0.342
TIMP-1	2.04 (1.08-3.85)	0.028	2.93 (1.12-7.65)	0.028
Plastin-2	1.57 (0.84-2.94)	0.156	2.49 (0.96-6.48)	0.062
REG3α	1.64 (0.88-3.08)	0.121	4.64 (1.55-13.89)	0.006

[a] Calcineurin inhibitor

[b] Methotrexate

[c] Mycophenolate

[d] Anti-thymocyte globulin

[e] Myeloablative conditioning

[f] Reduced-intensity conditioning

[g] Nonmyeloablative conditioning

aGVHD, acute graft-versus-host disease; NRM, non-relapse mortality; HR, hazard ratio; CI, confidence interval; alloHSCT, allogeneic hematopoietic stem cell transplantation; PBSC, peripheral blood stem cell; BM, bone marrow.

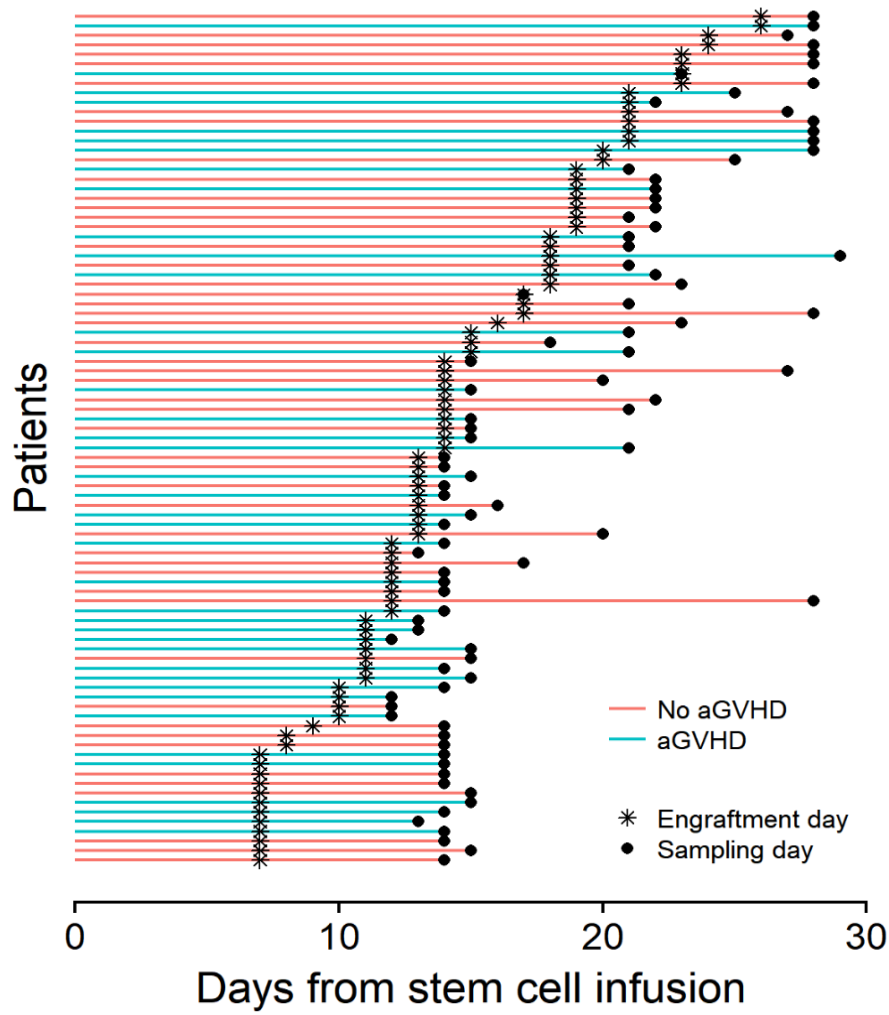

Figure 5. Days of engraftment and collection of plasma samples used in the verification set (n = 89).

Table 12. Adjusted association of the individual biomarker level with the risk of aGVHD

Variable	Model formula	HR (95% CI)	*P* value	AIC*
β2-microglobulin	Time to aGVHD ~ 1 + Prophylaxis + HLA match + β2-microglobulin	1.4 (0.73-2.68)	0.311	319.1
LRG	Time to aGVHD ~ 1 + Prophylaxis + Donor relationship + LRG	2.33 (1.18-4.61)	0.015	314.6
Fibrillin-like protein	Time to aGVHD ~ 1 + Prophylaxis + Donor relationship + Fibrillin-like protein	2.06 (1.04-4.07)	0.038	316.3
Peroxiredoxin-2	Time to aGVHD ~ 1 + Prophylaxis + HLA match + Peroxiredoxin-2	0.98 (0.5-1.92)	0.962	320.1
TIMP-1	Time to aGVHD ~ 1 + Prophylaxis + Donor relationship + TIMP-1	2.3 (1.19-4.46)	0.013	314.4
Plastin-2	Time to aGVHD ~ 1 + Prophylaxis + HLA match + Plastin-2	1.43 (0.74-2.77)	0.291	319
REG3α	Time to aGVHD ~ 1 + Prophylaxis + HLA match + REG3α	1.36 (0.69-2.7)	0.375	319.3

Table 13. Optimal multivariable Cox model for the risk of aGVHD with clinical characteristics only or with biomarkers added to the clinical characteristics

Variable	Clinical characteristics only		Clinical characteristics plus select biomarkers	
	HR (95% CI)	*P* value	HR (95% CI)	*P* value
HLA match: mismatched vs. matched	1.85 (0.96-3.55)	0.066	1.68 (0.87-3.25)	0.126
GVHD prophylaxis				
CNI + MTX/MMF vs. CNI alone	0.21 (0.09-0.49)	<0.001	0.2 (0.08-0.48)	<0.001
CNI + ATG ± MTX vs. CNI alone	0.26 (0.12-0.6)	0.001	0.35 (0.15-0.82)	0.015
Biomarkers: high vs. low				
TIMP-1	N/A	N/A	2.27 (1.15-4.5)	0.018
Plastin-2	N/A	N/A	1.73 (0.88-3.39)	0.11

aGVHD, acute graft-versus-host disease; HR, hazard ratio; CI, confidence interval; CNI, calcineurin inhibitor; MTX, methotrexate; MMF, mycophenolate mofetil; ATG, anti-thymocyte globulin.

Table 14. Adjusted association of the individual biomarker level with NRM

Variable	Model formula	HR (95% CI)	*P* value	AIC*
β2-microglobulin	NRM ~ 1 + Prophylaxis + Donor relationship + β2-microglobulin	2.55 (0.98-6.68)	0.056	157.1
LRG	NRM ~ 1 + Prophylaxis + Donor relationship + LRG	1.79 (0.71-4.5)	0.215	159.5
Fibrillin-like protein	NRM ~ 1 + Prophylaxis + Donor relationship + Fibrillin-like protein	2.05 (0.76-5.51)	0.157	159
Peroxiredoxin-2	NRM ~ 1 + Prophylaxis + Donor relationship + Peroxiredoxin-2	1.05 (0.41-2.69)	0.924	161
TIMP-1	NRM ~ 1 + Prophylaxis + Donor relationship + TIMP-1	2.99 (1.11-8.06)	0.031	156
Plastin-2	NRM ~ 1 + Prophylaxis + Donor relationship + Plastin-2	1.87 (0.7-5)	0.211	159.4
REG3α	NRM ~ 1 + Diagnosis + Donor relationship + REG3α	5.45 (1.79-16.62)	0.003	154.1

* Akaike Information Criterion

Table 15. Optimal multivariable Cox model for NRM with clinical characteristics only or with biomarkers added to the clinical characteristics

Variable	Clinical characteristics only		Clinical characteristics plus select biomarkers	
	HR (95% CI)	*P* value	HR (95% CI)	*P* value
Donor relationship: unrelated vs. related	3.81 (1.45-9.97)	0.006	4.54 (1.68-12.31)	0.003
GVHD prophylaxis				
CNI + MTX/MMF vs. CNI alone	0.22 (0.08-0.67)	0.007	0.4 (0.13-1.27)	0.122
CNI + ATG ± MTX vs. CNI alone	0.23 (0.08-0.67)	0.007	0.52 (0.17-1.56)	0.242
Biomarkers: high vs. low				
TIMP-1	N/A	N/A	2.65 (0.95-7.37)	0.062
Plastin-2	N/A	N/A	2.35 (0.86-6.42)	0.097
REG3α	N/A	N/A	3.32 (1.03-10.73)	0.045

NRM, non-relapse mortality; HR, hazard ratio; CI, confidence interval; GVHD, graft-versus-host disease; CNI, calcineurin inhibitor; MTX, methotrexate; MMF, mycophenolate mofetil; ATG, anti-thymocyte globulin.

Table 16. Association of the biomarker panel score with the risk of aGVHD and NRM

Model	Risk of aGVHD		NRM	
	HR* (95% CI)	*P* value	HR* (95% CI)	*P* value
Univariable	1.57 (1.13-2.18)	0.008	2.68 (1.57-4.59)	<0.001
Multivariable[a]	1.55 (1.07-2.25)	0.022	2.76 (1.52-4.99)	0.001

[a]The presented HR is adjusted for donor-recipient HLA allele match and GVHD prophylaxis regimens in the model for the risk of aGVHD and for donor-recipient relationship and GVHD prophylaxis regimens in the model for NRM as per the predefined variable selection algorithm.

* Cause-specific hazard ratio (CHR)

aGVHD, acute graft-versus-host disease; NRM, non-relapse mortality; HR, hazard ratio; CI, confidence interval.

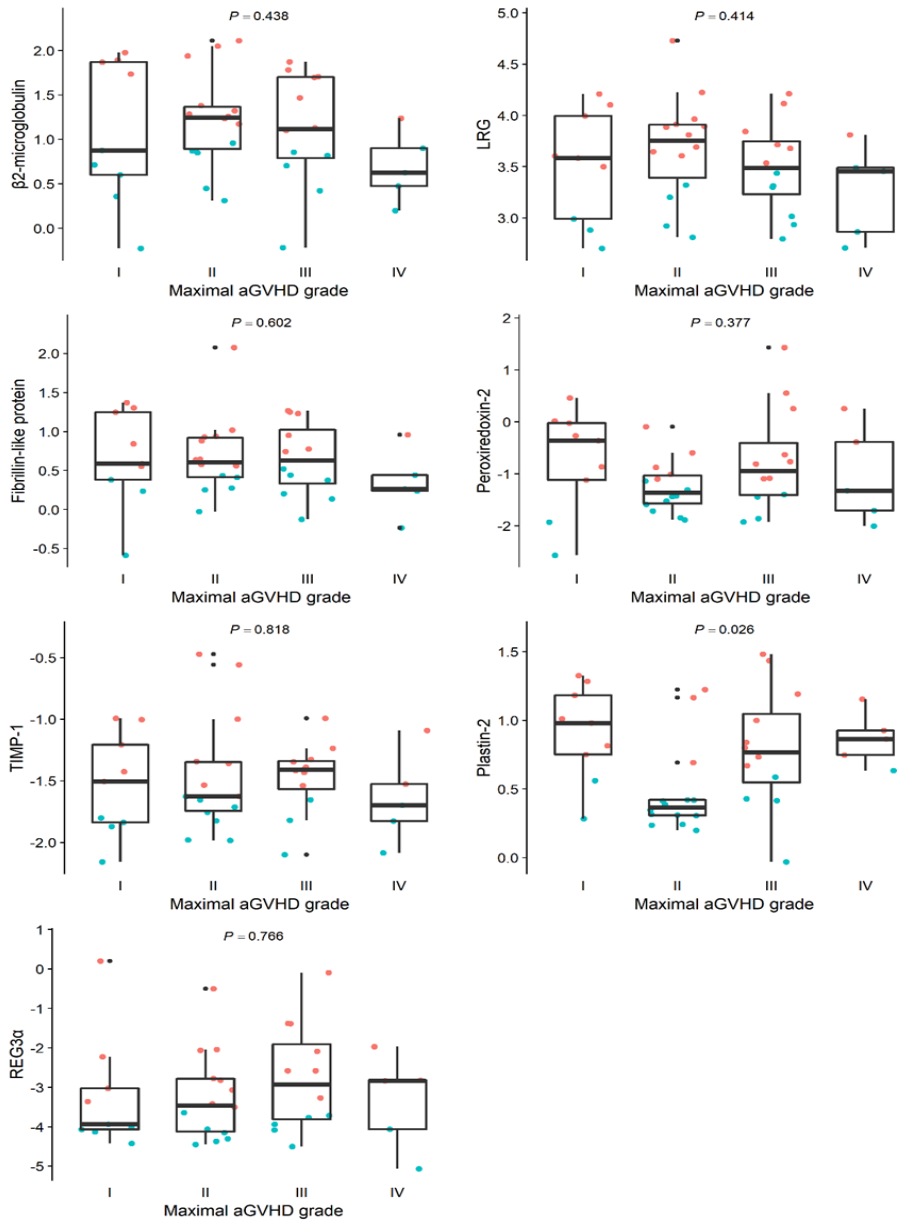

Figure 6. Comparison of relationship between the biomarker candidate level and the maximal grade of aGVHD for 40 patients who developed aGVHD. Red and blue dot indicate ‘high’ and ‘low’ level groups respectively.

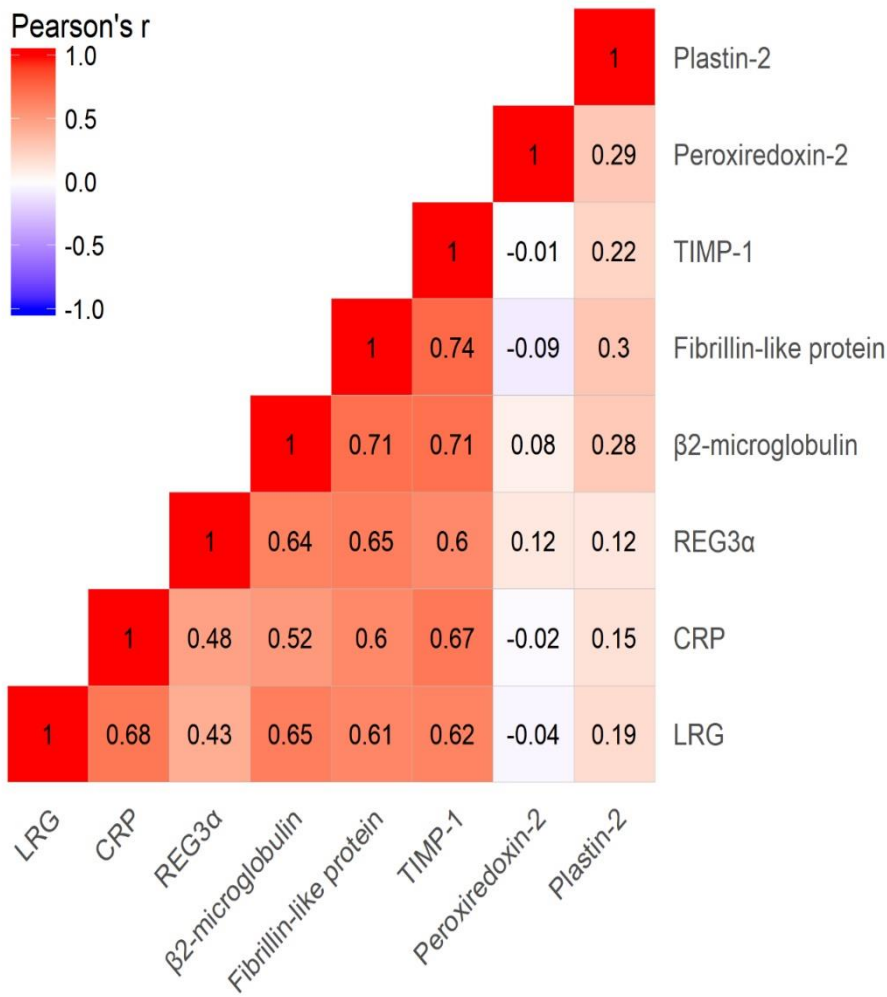

Figure 7. Pairwise correlation of the plasma level of candidate protein biomarkers in the verification set (n = 89)

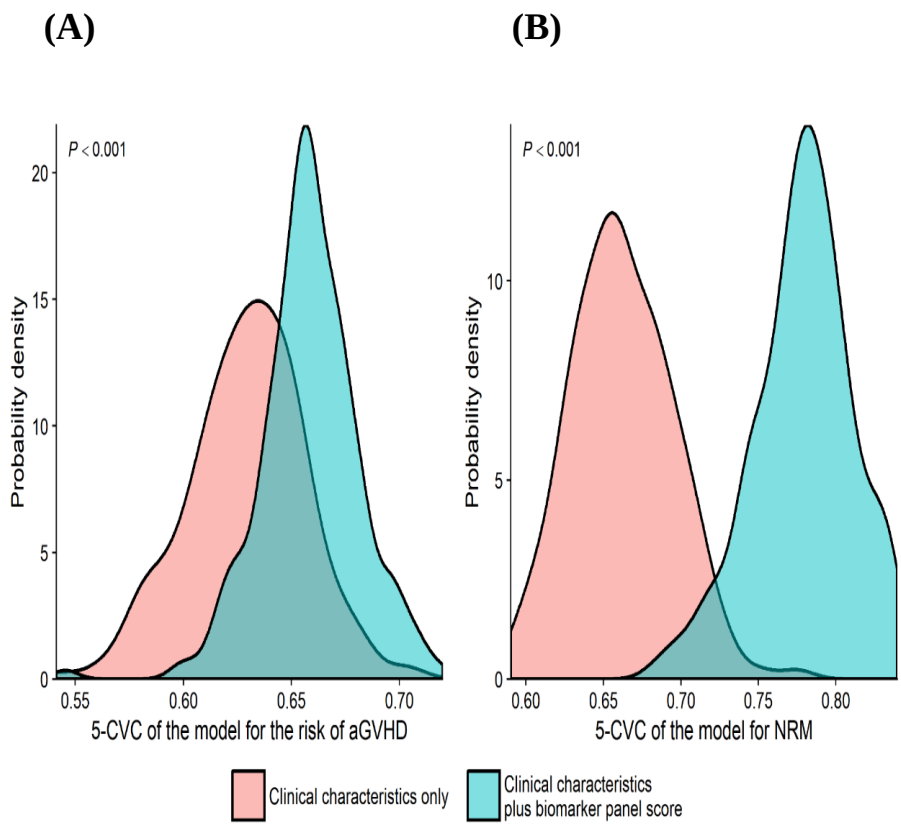

Figure 8. Distribution of five-fold cross-validated Harrell's C (5-CVC) for the risk of aGVHD (left panel) and NRM (right panel), X axis: Harrell's C, Y axis: Distribution of Harrell's C (5-CVC) generated using 200 independent random splitting of verification set into five subsets for the Cox model containing clinical characteristics only and the Cox model containing clinical characteristics plus biomarker panel score.

(A): Distribution of five-fold cross-validated Harrell's C (5-CVC) for the risk of aGVHD.

(B): Distribution of five-fold cross-validated Harrell's C (5-CVC) for the NRM

Table 17. Reclassification of the risk of aGVHD after adding the biomarker panel score to the clinical predictors in the Cox model

Variable	Patients who developed aGVHD within 6 months after alloHSCT	Patients who did not develop aGVHD within 6 months after alloHSCT
KM-estimated number of patients, n	38.6	50.4
Reclassified to higher risk, n (%)	25.6 (66.4)	22.4 (44.4)
Reclassified to lower risk, n (%)	14.2 (36.8)	26.8 (53.2)
Net reclassification improvement (%)	29.6	8.8
P value	0.074	

aGVHD, acute graft-versus-host disease; NRM, non-relapse mortality; KM, Kaplan-Meier.

Table 18. Reclassification of NRM after adding the biomarker panel score to the clinical predictors in the Cox model

Variable	Patients who died without relapse within 1 year after alloHSCT	Patients who did not die without relapse within 1 year after alloHSCT
KM-estimated number of patients, n	18.1	70.9
Reclassified to higher risk, n (%)	12.1 (67)	27.9 (39.3)
Reclassified to lower risk, n (%)	6.2 (34.4)	42.8 (60.3)
Net reclassification improvement (%)	32.7	21
P value	0.032	

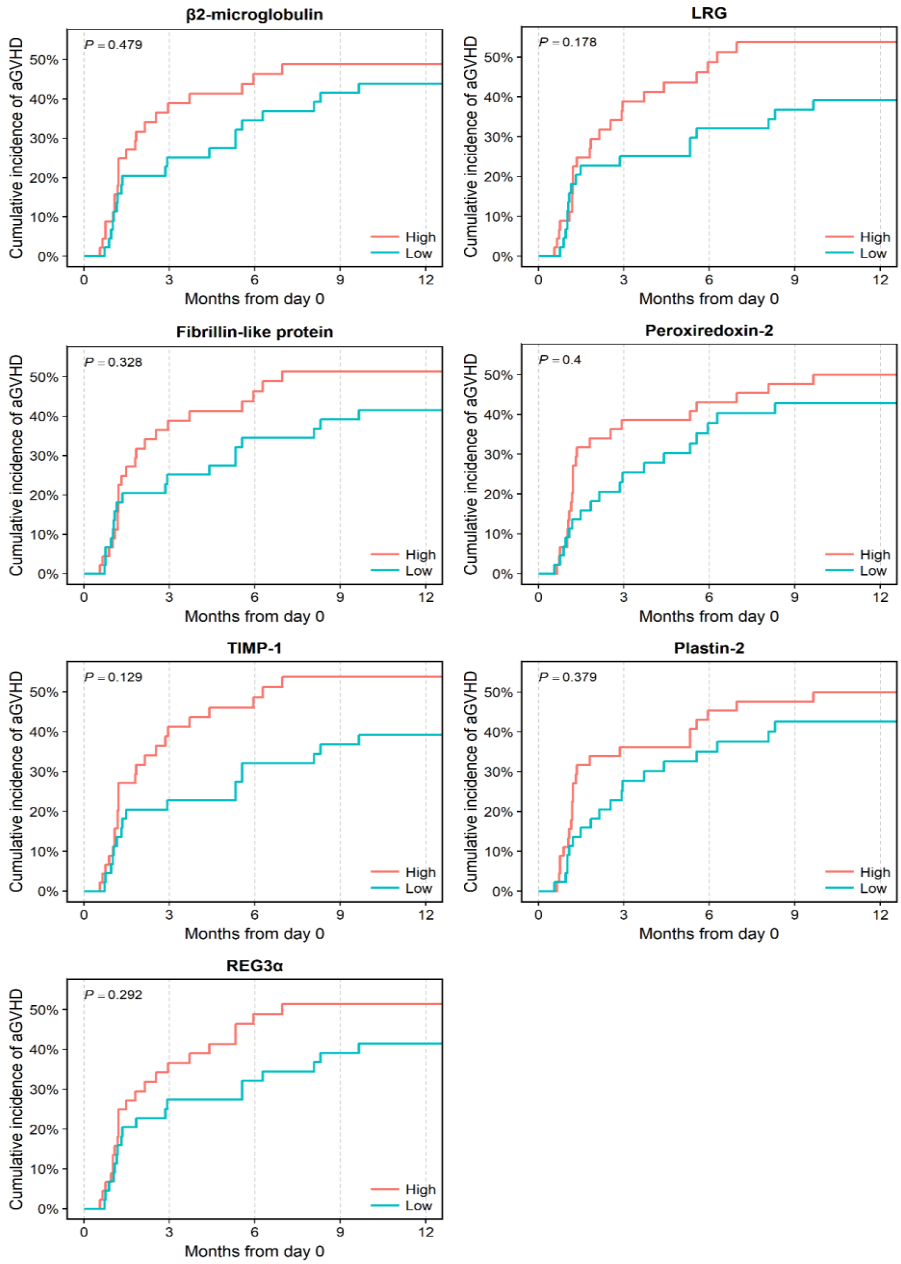

Figure 9. Comparison of cumulative incidence for aGVHD according to high and low plasma level of each candidate biomarker

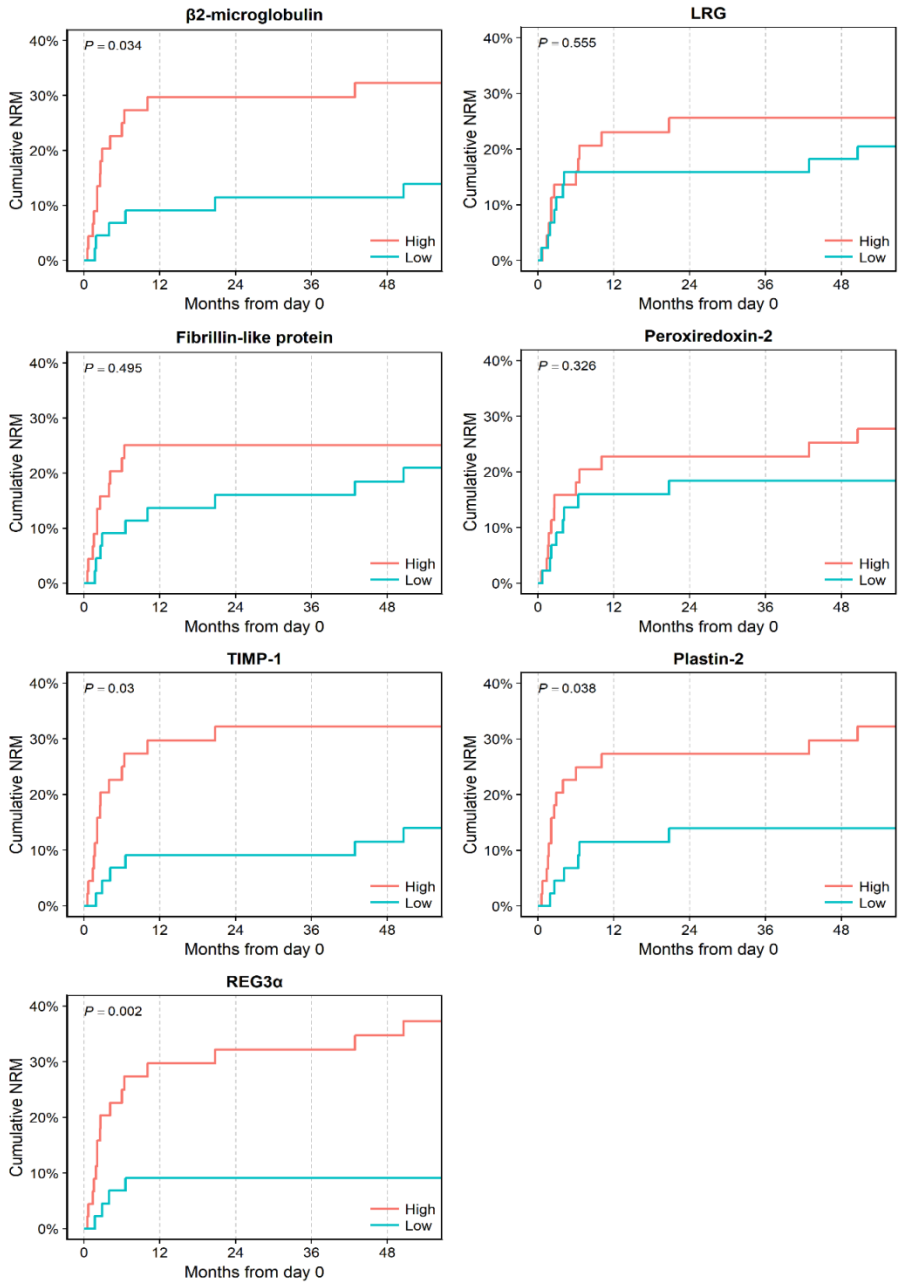

Figure 10. Comparison of cumulative incidence of NRM according to high and low plasma level of each candidate biomarker

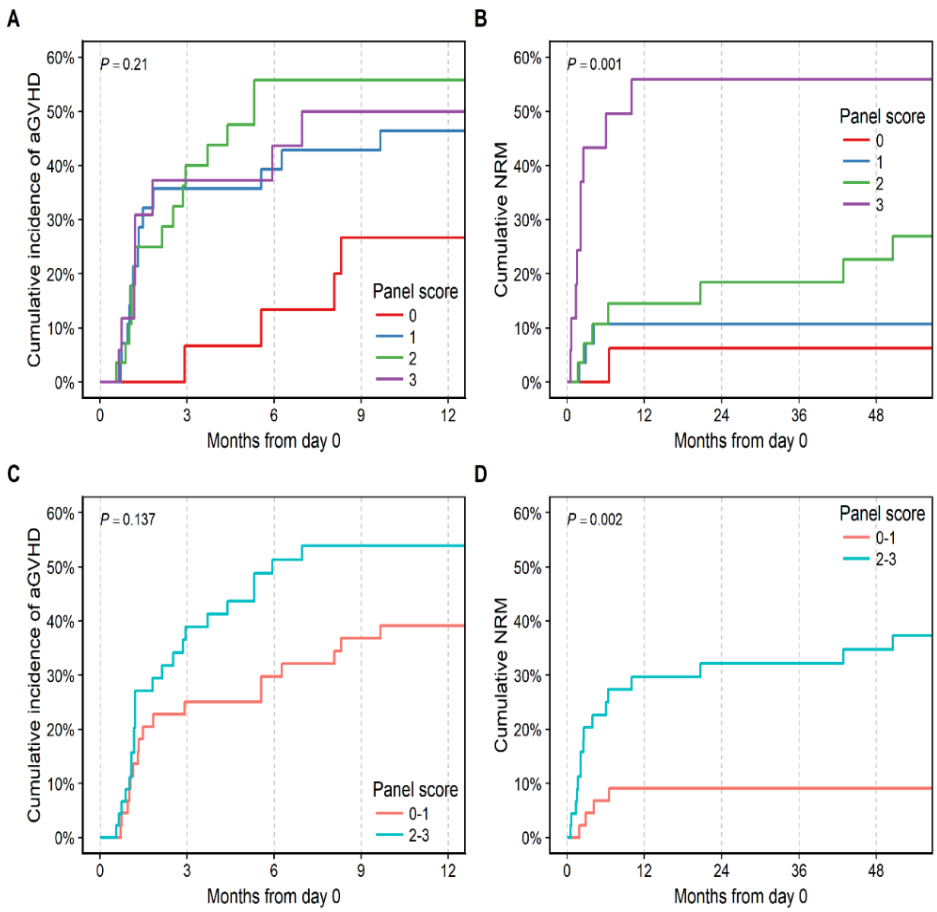

Figure 11. Cumulative incidence of aGVHD (A and C) and NRM (B and D) according to the biomarker panel score.

aGVHD, acute graft-versus-host disease; NRM, non-relapse mortality

Table 19. Association of the biomarker panel score with the Fine-Gray subdistribution hazards of aGVHD and NRM

Model	Risk of aGVHD		NRM	
	HR* (95% CI)	*P* value	HR* (95% CI)	*P* value
Univariable	1.3 (0.98-1.71)	0.068	2.68 (1.52-4.74)	0.001
Multivariable[a]	1.2 (0.85-1.69)	0.29	2.56 (1.36-4.81)	0.003

[a] The presented HR is adjusted for donor-recipient HLA allele match and GVHD prophylaxis regimens in the model for the risk of aGVHD and for donor-recipient relationship and GVHD prophylaxis regimens in the model for NRM as per the predefined variable selection algorithm.

* Subdistribution hazard ratio

aGVHD, acute graft-versus-host disease; NRM, non-relapse mortality; HR, hazard ratio; CI, confidence interval

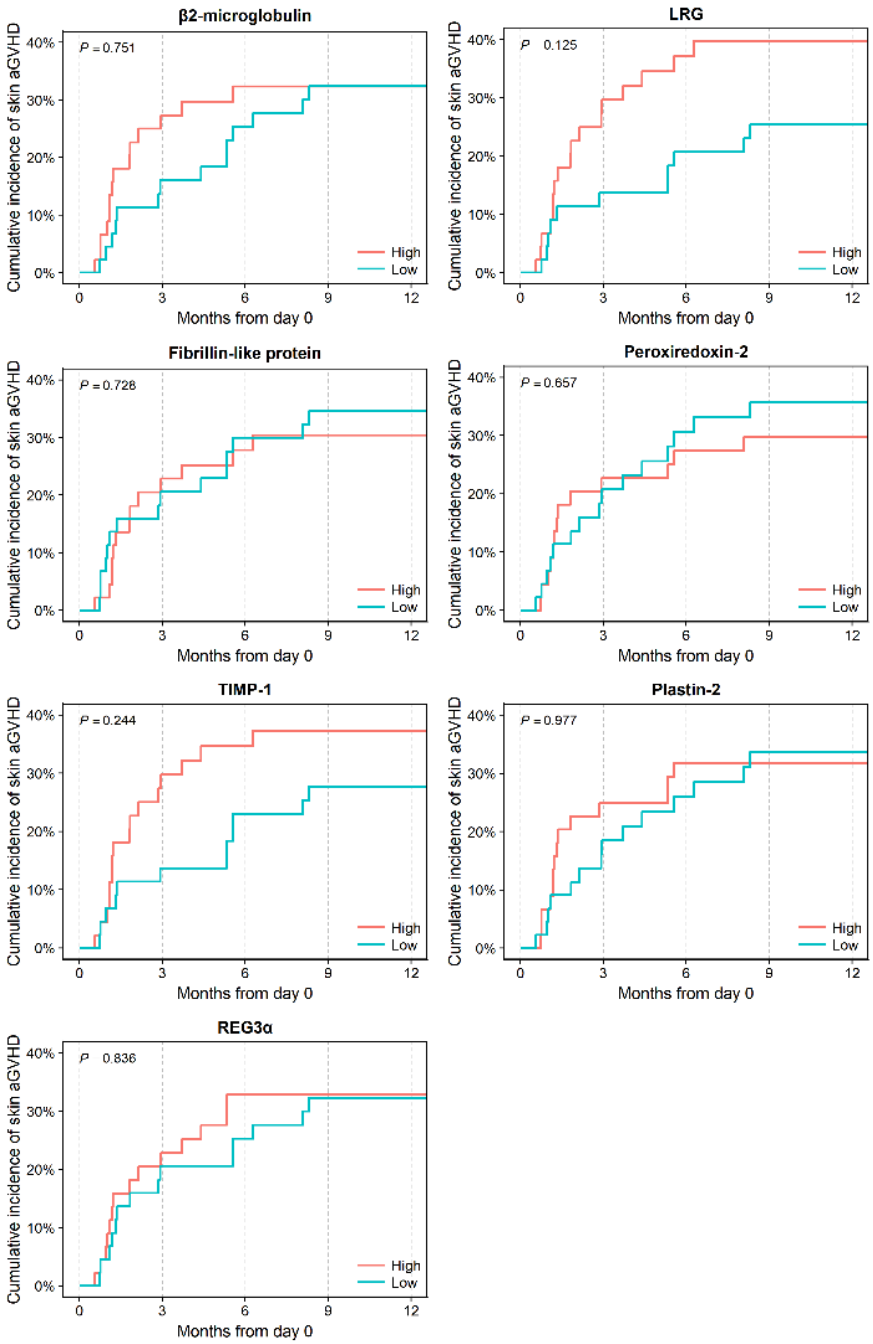

Figure 12. Comparison of cumulative incidence for skin aGVHD according to high and low plasma level of each candidate biomarker

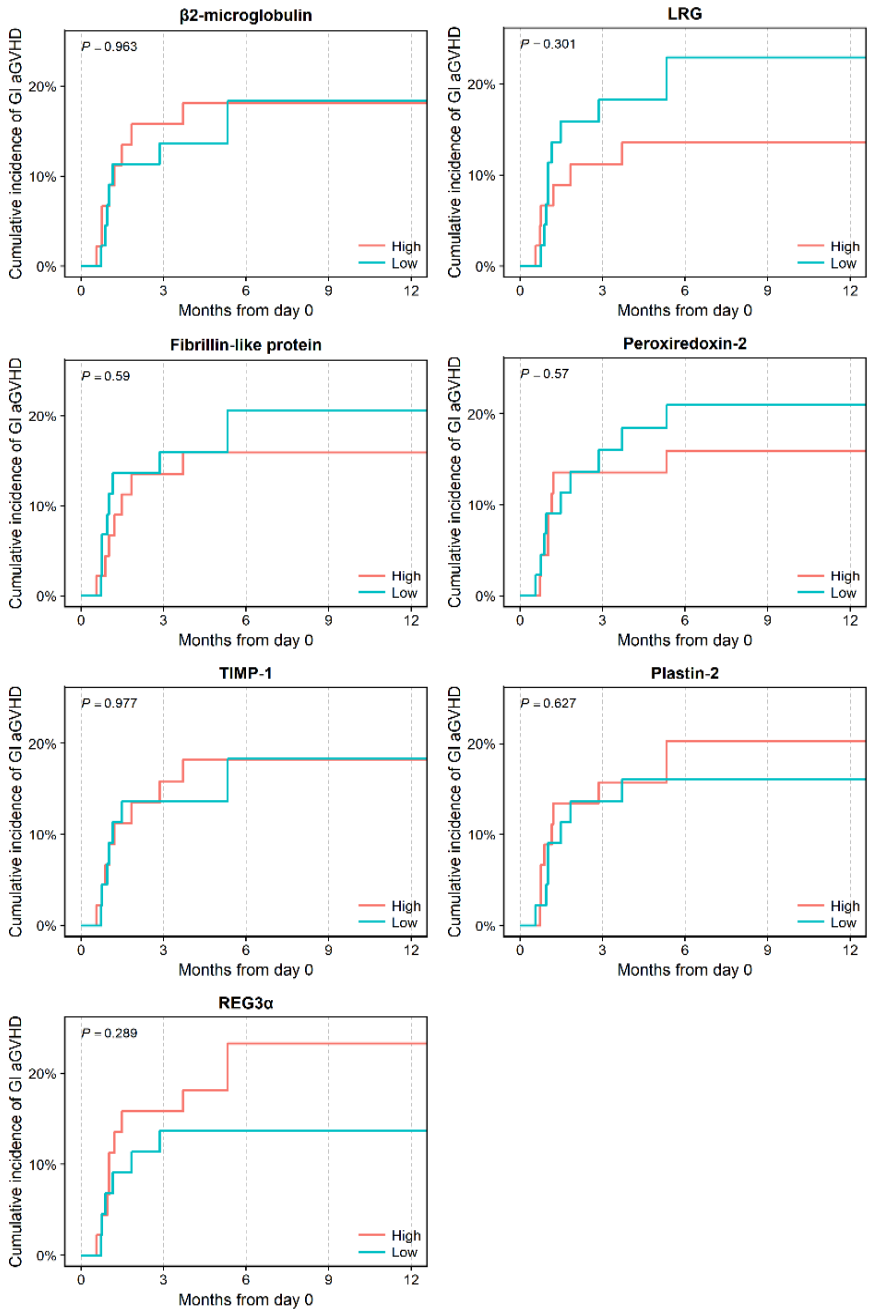

Figure 13. Comparison of cumulative incidence for GI (gastrointestinal tract) aGVHD according to high and low plasma level of each candidate biomarker

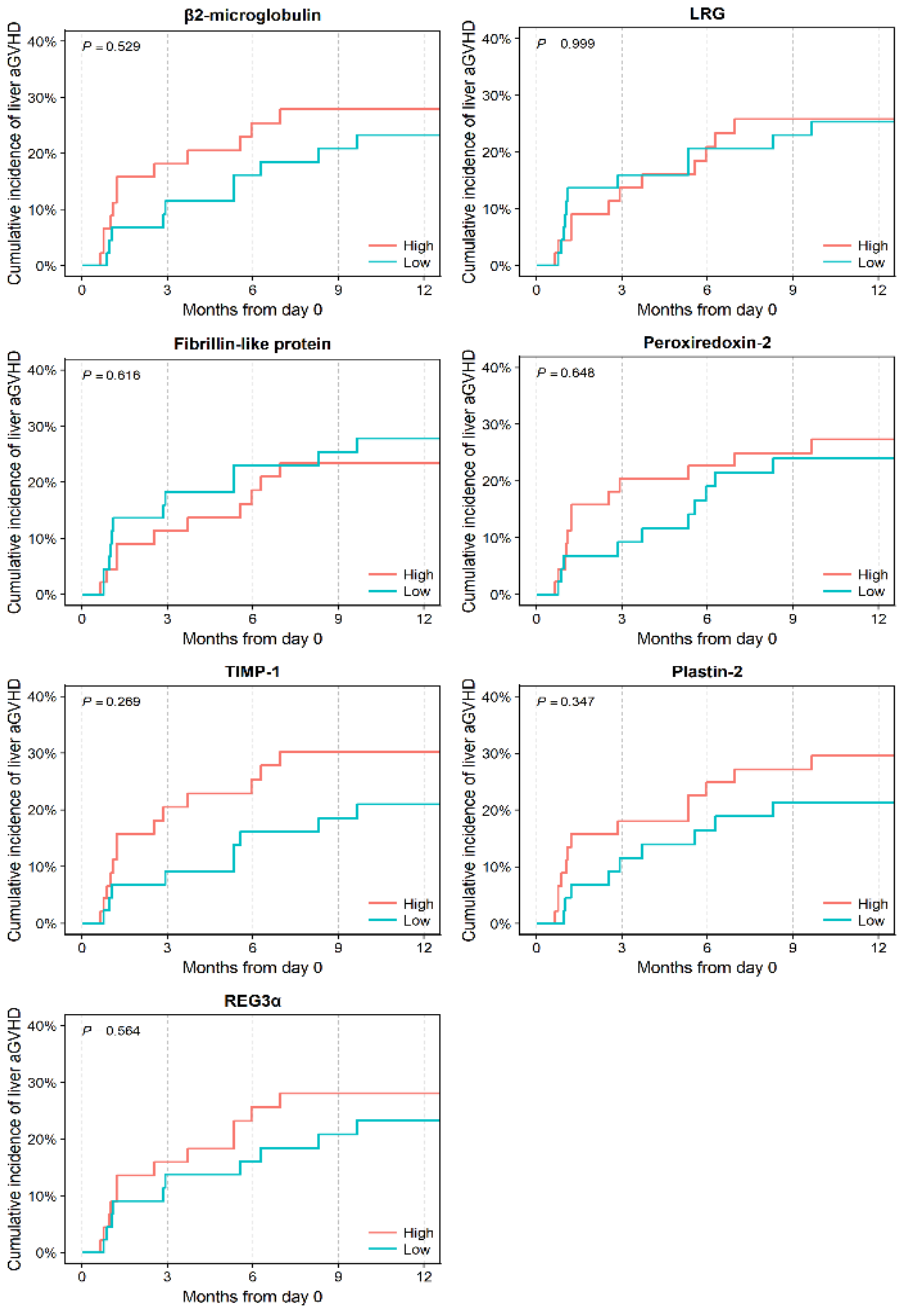

Figure 14. Comparison of cumulative incidence for liver aGVHD according to high and low plasma level of each candidate biomarker

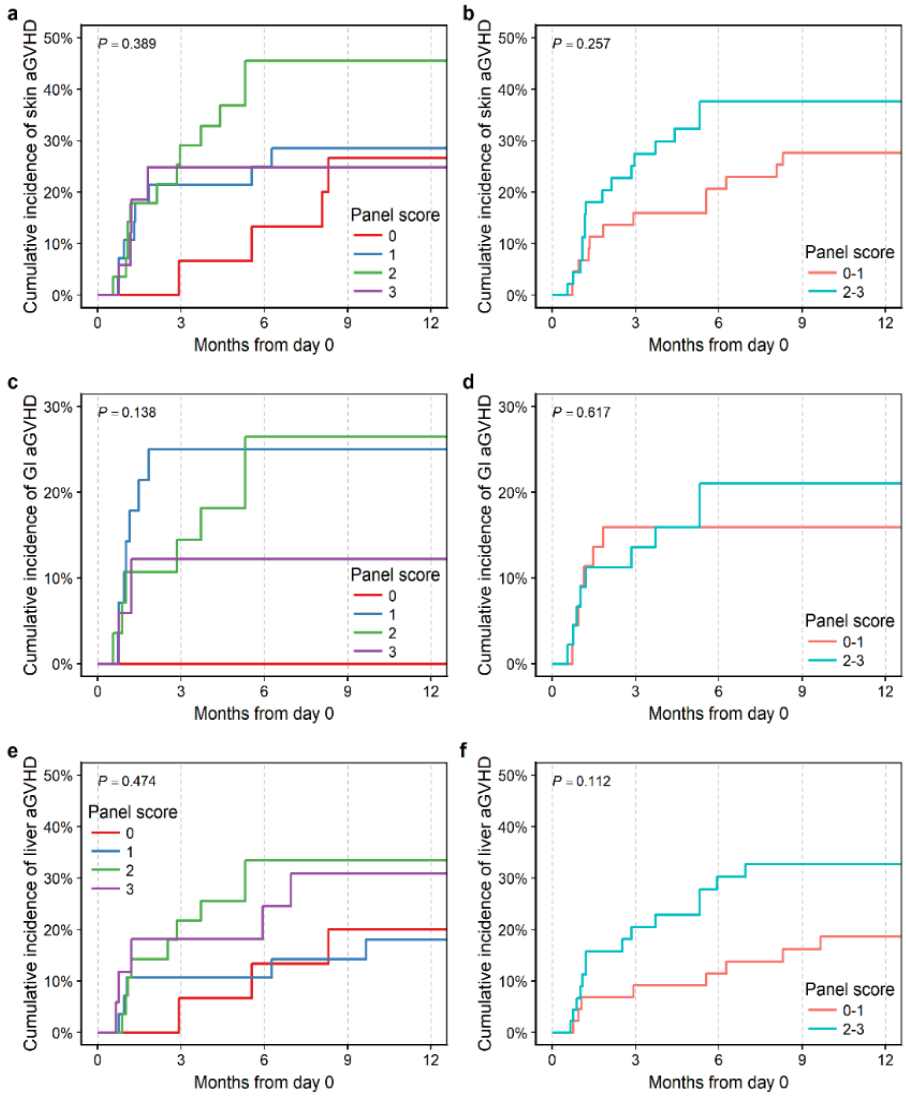

Figure 15. Comparison of cumulative incidence for three types of organ-specific aGVHD, i.e., skin (panels a and b), gastrointestinal tract (panels c and d), and liver (panels e and f), according to the biomarker panel score

4. Discussion

In this study, I used a nanoLC-MS based label-free quantitative proteomics method for comprehensive proteome profiling of plasma samples from aGVHD and control patients who underwent alloHSCT in the discovery set and verified the predictive value of seven candidate biomarkers in post-engraftment plasma samples of an independent patient cohort in terms of the risk for aGVHD and NRM. I verified three biomarker candidates, i.e., TIMP-1, plastin-2, and REG3α, which were used in combination to develop a simple biomarker panel score that accurately and precisely stratified patients according to the risk of aGVHD and NRM post-alloHSCT. I also demonstrated that adding the biomarker panel score to established clinical predictors significantly improved the discriminatory performance of the Cox model in predicting the risk of aGVHD and NRM. Because aGVHD represents a main cause of NRM in patients undergoing alloHSCT, it is clinically plausible that the predictive value of biomarkers for aGVHD risk directly translates into their predictive value for NRM.

Only some of the selected biomarkers showed significant values when analyzed individually, while the biomarker panel score was significantly correlated with both aGVHD risk and NRM. Given the heterogeneity and complexity in the aGVHD pathophysiology, it is unlikely that a single protein represents the overall pathogenesis of aGVHD [1]. Instead, combining multiple biomarkers into a panel-based scoring system may be a more promising strategy. Indeed, a series of previous studies demonstrated that by combining multiple biomarkers into a panel-based prediction model, patients with and without aGVHD were successfully discriminated and the risk of unresponsiveness to corticosteroid therapy and subsequent NRM were predicted in

patients who developed aGVHD following alloHSCT [6,7,8]. In the present study, I extended the clinical utility of the plasma-based biomarker panel by demonstrating that it can also be used to predict the risk of aGVHD and NRM even before the onset of clinical manifestations.

Notably, the HR for NRM was higher than that for the risk of aGVHD in both Cox model and Fine-Gray model analyses, suggesting an additional role for the biomarker panel score in predicting aGVHD-unrelated NRM. In line with this reasoning, the Fine-Gray model for death without aGVHD indicated that the biomarker panel score was correlated more strongly with the incidence of aGVHD-unrelated death than with the incidence of aGVHD itself. Therefore, the effect of the biomarker panel score on the cumulative incidence of aGVHD was likely negatively affected by its stronger effect on the risk of a competing event, i.e., death without aGVHD, resulting in an attenuated subdistribution HR for aGVHD in the Fine-Gray model. This is commonly observed in competing risks studies [56,57]. However, we cannot exclude the possibility that our competing-risk model analysis was not sufficiently empowered to detect the predictive association of the biomarker panel score with the incidence of aGVHD because of the relatively small number of patients in the verification set.

Among the three biomarkers included in the panel score, REG3α is widely known as a gastrointestinal aGVHD-specific marker [42,43]. REG3α is a C-type lectin protein secreted by Paneth cells and mediates antibacterial mechanisms in the intestinal crypt microenvironment downstream of interleukin-22 regulation [44,54]. Since its discovery, studies using REG3α in systemic aGVHD biomarker panels have shown promising results [7,8]. Visual comparison of the cumulative incidence curves for gastrointestinal aGVHD between patients with high and low levels of plasma REG3α indicated the

potential predictive value of this protein for intestinal aGVHD in our study. Given that this study was not statistically empowered to draw reliable target organ-specific results, the predictive role of plasma REG3α for intestinal aGVHD should be confirmed in future studies. TIMP-1 belongs to a family of four endogenous metalloproteinase inhibitors (TIMP-1–4) that are involved in a broad range of biological activities [45]. Over the last several decades, growing evidence has provided insight into the fundamental roles of matrix metalloproteinases and their endogenous inhibitors including TIMP-1 in immune regulation [46]. Accordingly, dysregulation in their activity has been linked to various inflammatory and autoimmune disorders such as inflammatory bowel disease, granulomatous skin disorder, and aGVHD [46,47]. Furthermore, previous studies showed that a synthetic metalloproteinase inhibitor significantly ameliorated the phenotypic and pathologic severity of aGVHD and mortality in animal models [48,49]. Therefore, although TIMP-1 was not previously evaluated for its predictive or prognostic role, theoretical information and evidence from research indicate that it is a plausible biomarker for aGVHD. The last protein comprising the biomarker panel score, plastin-2, is an actin-binding protein that mediates the transport of the T cell activation molecules CD25 and CD69 to the cell surface in response to costimulation through T cell receptor/CD3 plus CD2 or CD28 [50]. Plastin-2 governs the bundling of the F-actin cytoskeleton, which is crucial for immunological synapse formation, polarization, and migration in chemokine-stimulated T cells [51,52]. Importantly, costimulation-induced plastin-2 phosphorylation at serine residues is inhibited by the glucocorticoid dexamethasone, which consequently prevents maturation of the immune synapse [55]. Therefore, the anti-aGVHD mechanisms of the glucocorticoid may at least in part be explained by its

inhibitory effect on plastin-2-mediated immune synapse formation. Together, these observations emphasize the key role of plastin-2 in activating T cells that coordinate aGVHD pathogenesis. Nevertheless, it remains unclear how plastin-2 is released into the plasma during the early post-alloHSCT period and how its plasma level is related to alloimmune activity.

This study had some limitations. First and most importantly, I could not externally validate the predictive value of the biomarker panel score because of a lack of an additional independent cohort. Although we employed an alternative strategy using internal validation methods such as 5-fold cross-validation and bootstrap, this is not sufficient for the development of a new prediction model. Additionally, the small size of our verification set did not enable determination of the organ-specific association of each biomarker. For the same reason, we could not assess whether the identified biomarkers are specific for aGVHD or also indicative of other alloHSCT-related complications such as infection or veno-occlusive disease. The lack of association between the candidate biomarker levels and clinical grade of aGVHD also limited the interpretation. Finally, although the biomarker panel score defined in this study is intuitive and easy-to-implement, the optimal thresholds for dividing patients into the high-level and low-level groups should be determined using a larger number of cases.
Despite these limitations, to the best of my knowledge, this is the first study employing an nanoLC-MS based proteome profiling method for the discovery of target proteins and LC-MRM-MS-based quantification method for verification of target proteins, which is currently a state-of-the-art method in proteomics research, to develop a predictive plasma-based biomarker panel for aGVHD using samples obtained during the preclinical stage. The results indicated a consistent tendency toward higher aGVHD

risk and NRM in patients with high levels of seven candidate biomarkers. The three-protein biomarker panel enabled prediction of the risk of aGVHD and NRM independently of clinical characteristics and significantly improved model performance. Another important clinical implication of GVHD-specific biomarkers is that they can be targeted therapeutically, as exemplified by the metalloproteinase inhibitor and tumor necrosis factor blockade [48,49,53]. Therefore, continuing efforts to identify a comprehensive catalogue of aGVHD biomarkers may enable the development of novel prophylactic and therapeutic agents.

5. References

1. Blazar BR, Murphy WJ, Abedi M. Advances in graft-versus-host disease biology and therapy. Nat Rev Immunol. 2012;12(6):443-58.

2. Ferrara JLM, Levine JE, Reddy P, Holler E. Graft-versus-host disease. The Lancet. 2009;373(9674):1550-61.

3. Garnett C, Apperley JF, Pavlu J. Treatment and management of graft-versus-host disease: improving response and survival. Ther Adv Hematol. 2013;4(6):366-78.

4. Sorror ML, Sandmaier BM, Storer BE, Maris MB, Baron F, Maloney DG, et al. Comorbidity and disease status based risk stratification of outcomes among patients with acute myeloid leukemia or myelodysplasia receiving allogeneic hematopoietic cell transplantation. J Clin Oncol. 2007;25(27):4246-54.

5. Paczesny S. Discovery and validation of graft-versus-host disease biomarkers. Blood. 2013;121(4):585-94.

6. Paczesny S, Krijanovski OI, Braun TM, Choi SW, Clouthier SG, Kuick R, et

al. A biomarker panel for acute graft-versus-host disease. Blood. 2009;113(2):273-8.

7. Levine JE, Logan BR, Wu J, Alousi AM, Bolanos-Meade J, Ferrara JL, et al. Acute graft-versus-host disease biomarkers measured during therapy can predict treatment outcomes: a Blood and Marrow Transplant Clinical Trials Network study. Blood. 2012;119(16):3854-60.

8. Levine JE, Braun TM, Harris AC, Holler E, Taylor A, Miller H, et al. A prognostic score for acute graft-versus-host disease based on biomarkers: a multicentre study. The Lancet Haematology. 2015;2(1):e21-e9.

9. Vander Lugt MT, Braun TM, Hanash S, Ritz J, Ho VT, Antin JH, et al. ST2 as a marker for risk of therapy-resistant graft-versus-host disease and death. N Engl J Med. 2013;369(6):529-39.

10. Levine JE, Paczesny S, Sarantopoulos S. Clinical applications for biomarkers of acute and chronic graft-versus-host disease. Biology of Blood and Marrow Transplantation. 2012;18(1):S116-S24.

11. Weissinger EM, Schiffer E, Hertenstein B, Ferrara JL, Holler E, Stadler M, et al. Proteomic patterns predict acute graft-versus-host disease after allogeneic hematopoietic stem cell transplantation. Blood. 2007;109(12):5511-9.

12. Choi SW, Stiff P, Cooke K, Ferrara JL, Braun T, Kitko C, et al. TNF-inhibition with etanercept for graft-versus-host disease prevention in high-risk HCT: lower TNFR1 levels correlate with better outcomes. Biol Blood Marrow Transplant. 2012;18(10):1525-32.

13. Paczesny S, Braun T, Vander Lugt M, Harris A, Fiema B, Hernandez J, et al. A Three Biomarker Panel at Days 7 and 14 Can Predict Development of Grade II-IV Acute Graft-Versus-Host Disease. Biology of Blood and Marrow Transplantation. 2011;17(2).

14. Cominetti O, Nunez Galindo A, Corthesy J, Oller Moreno S, Irincheeva I, Valsesia A, et al. Proteomic Biomarker Discovery in 1000 Human Plasma Samples with Mass Spectrometry. J Proteome Res. 2016;15(2):389-99.

15. Sogawa K, Takano S, Iida F, Satoh M, Tsuchida S, Kawashima Y, et al. Identification of a novel serum biomarker for pancreatic cancer, C4b-binding protein alpha-chain (C4BPA) by quantitative proteomic analysis using tandem mass tags. Br J Cancer. 2016;115(8):949-56.

16. Kim Y, Jeon J, Mejia S, Yao CQ, Ignatchenko V, Nyalwidhe JO, et al. Targeted proteomics identifies liquid-biopsy signatures for extracapsular prostate cancer. Nat Commun. 2016;7:11906.

17. Kim JY, Lee H, Woo J, Yue W, Kim K, Choi S, et al. Reconstruction of pathway modification induced by nicotinamide using multi-omic network analyses in triple negative breast cancer. Sci Rep. 2017;7(1):3466.

18. Füzéry AK, Levin J, Chan MM, Chan DW. Translation of proteomic biomarkers into FDA approved cancer diagnostics: issues and challenges. Clinical proteomics. 2013;10(1):13.

19. Parker CE, Borchers CH. Mass spectrometry based biomarker discovery, verification, and validation--quality assurance and control of protein biomarker assays. Mol Oncol. 2014;8(4):840-58.

20. Gillette MA, Carr SA. Quantitative analysis of peptides and proteins in biomedicine by targeted mass spectrometry. Nat Methods. 2013;10(1):28-34.

21. Carr SA, Abbatiello SE, Ackermann BL, Borchers C, Domon B, Deutsch EW, et al. Targeted peptide measurements in biology and medicine: best practices for mass spectrometry-based assay development using a fit-for-purpose approach. Mol Cell Proteomics. 2014;13(3):907-17.

22. Abbatiello SE, Schilling B, Mani DR, Zimmerman LJ, Hall SC, MacLean B, et al. Large-Scale Interlaboratory Study to Develop, Analytically Validate and Apply Highly Multiplexed, Quantitative Peptide Assays to Measure Cancer-Relevant Proteins in Plasma. Mol Cell Proteomics. 2015;14(9):2357-74.

23. Kennedy JJ, Abbatiello SE, Kim K, Yan P, Whiteaker JR, Lin C, et al. Demonstrating the feasibility of large-scale development of standardized assays to quantify human proteins. Nat Methods. 2014;11(2):149-55.

24. Uzozie AC, Selevsek N, Wahlander A, Nanni P, Grossmann J, Weber A, et al. Targeted Proteomics for Multiplexed Verification of Markers of Colorectal Tumorigenesis. Mol Cell Proteomics. 2017;16(3):407-27.

25. Lopez MF, Kuppusamy R, Sarracino DA, Prakash A, Athanas M, Krastins B, et al. Mass spectrometric discovery and selective reaction monitoring (SRM) of putative protein biomarker candidates in first trimester Trisomy 21 maternal serum. Journal of proteome research. 2010;10(1):133-42.

26. Przepiorka D, Weisdorf D, Martin P, Klingemann H, Beatty P, Hows J, et al. 1994 Consensus conference on acute GVHD grading. Bone marrow transplantation. 1995;15(6):825-8.

27. Geromanos SJ, Vissers JP, Silva JC, Dorschel CA, Li GZ, Gorenstein MV, et al. The detection, correlation, and comparison of peptide precursor and product ions from data independent LC-MS with data dependant LC-MS/MS. Proteomics. 2009;9(6):1683-95.

28. Li GZ, Vissers JP, Silva JC, Golick D, Gorenstein MV, Geromanos SJ. Database searching and accounting of multiplexed precursor and product ion spectra from the data independent analysis of simple and complex peptide mixtures. Proteomics. 2009;9(6):1696-719.

29. Silva JC, Gorenstein MV, Li GZ, Vissers JP, Geromanos SJ. Absolute quantification of proteins by LCMSE: a virtue of parallel MS acquisition. Mol Cell Proteomics. 2006;5(1):144-56.

30. Kramer G, Woolerton Y, van Straalen JP, Vissers JP, Dekker N, Langridge JI, et al. Accuracy and Reproducibility in Quantification of Plasma Protein Concentrations by Mass Spectrometry without the Use of Isotopic Standards. PLoS One. 2015;10(10):e0140097.

31. MacLean B, Tomazela DM, Shulman N, Chambers M, Finney GL, Frewen B, et al. Skyline: an open source document editor for creating and analyzing targeted proteomics experiments. Bioinformatics. 2010;26(7):966-8.

32. Mani DR, Abbatiello SE, Carr SA. Statistical characterization of multiple-reaction monitoring mass spectrometry (MRM-MS) assays for quantitative proteomics. BMC Bioinformatics. 2012;13 Suppl 16:S9.

33. Currie LA. Limits for qualitative detection and quantitative determination. Application to radiochemistry. Analytical chemistry. 1968;40(3):586-93.

34. Calcagno V, de Mazancourt C. glmulti: an R package for easy automated model selection with (generalized) linear models. Journal of statistical software. 2010;34(12):1-29.

35. Pencina MJ, D'Agostino RB. Overall C as a measure of discrimination in survival analysis: model specific population value and confidence interval estimation. Stat Med. 2004;23(13):2109-23.

36. Pencina MJ, D'Agostino RB, Sr., Steyerberg EW. Extensions of net reclassification improvement calculations to measure usefulness of new biomarkers. Stat Med. 2011;30(1):11-21.

37. Gray RJ. A class of K-sample tests for comparing the cumulative incidence of

a competing risk. The Annals of statistics. 1988:1141-54.

38. Fine JP, Gray RJ. A proportional hazards model for the subdistribution of a competing risk. Journal of the American statistical association. 1999;94(446):496-509.

39. Bogdanow B, Zauber H, Selbach M. Systematic Errors in Peptide and Protein Identification and Quantification by Modified Peptides. Mol Cell Proteomics. 2016;15(8):2791-801.

40. Proc JL, Kuzyk MA, Hardie DB, Yang J, Smith DS, Jackson AM, et al. A quantitative study of the effects of chaotropic agents, surfactants, and solvents on the digestion efficiency of human plasma proteins by trypsin. J Proteome Res. 2010;9(10):5422-37.

41. Paczesny S, Braun TM, Levine JE, Hogan J, Crawford J, Coffing B, et al. Elafin is a biomarker of graft-versus-host disease of the skin. Sci Transl Med. 2010;2(13):13ra2.

42. Ferrara JL, Harris AC, Greenson JK, Braun TM, Holler E, Teshima T, et al. Regenerating islet-derived 3-alpha is a biomarker of gastrointestinal graft-versus-host disease. Blood. 2011;118(25):6702-8.

43. Harris AC, Ferrara JL, Braun TM, Holler E, Teshima T, Levine JE, et al. Plasma biomarkers of lower gastrointestinal and liver acute GVHD. Blood. 2012;119(12):2960-3.

44. Zheng Y, Valdez PA, Danilenko DM, Hu Y, Sa SM, Gong Q, et al. Interleukin-22 mediates early host defense against attaching and effacing bacterial pathogens. Nat Med. 2008;14(3):282-9.

45. Brew K, Nagase H. The tissue inhibitors of metalloproteinases (TIMPs): an ancient family with structural and functional diversity. Biochim Biophys Acta. 2010;1803(1):55-71.

46. Khokha R, Murthy A, Weiss A. Metalloproteinases and their natural inhibitors in inflammation and immunity. Nat Rev Immunol. 2013;13(9):649-65.

47. Salmela MT, Karjalainen-Lindsberg ML, Jeskanen L, Saarialho-Kere U. Overexpression of tissue inhibitor of metalloproteinases-3 in intestinal and cutaneous lesions of graft-versus-host disease. Mod Pathol. 2003;16(2):108-14.

48. Hattori K, Hirano T, Ushiyama C, Miyajima H, Yamakawa N, Ebata T, et al. A metalloproteinase inhibitor prevents lethal acute graft-versus-host disease in mice. Blood. 1997;90(2):542-8.

49. Hattori K, Hirano T, Oshimi K, Yagita H, Okumura K. A metalloproteinase inhibitor prevents acute graft-versus-host disease while preserving the graft-versus-leukaemia effect of allogeneic bone marrow transplantation. Leuk Lymphoma. 2000;38(5-6):553-61.

50. Wabnitz GH, Kocher T, Lohneis P, Stober C, Konstandin MH, Funk B, et al. Costimulation induced phosphorylation of L-plastin facilitates surface transport of the T cell activation molecules CD69 and CD25. Eur J Immunol. 2007;37(3):649-62.

51. Wang C, Morley SC, Donermeyer D, Peng I, Lee WP, Devoss J, et al. Actin-bundling protein L-plastin regulates T cell activation. J Immunol. 2010;185(12):7487-97.

52. Freeley M, O'Dowd F, Paul T, Kashanin D, Davies A, Kelleher D, et al. L-plastin regulates polarization and migration in chemokine-stimulated human T lymphocytes. J Immunol. 2012;188(12):6357-70.

53. Choi SW, Stiff P, Cooke K, Ferrara JL, Braun T, Kitko C, et al. TNF-inhibition with etanercept for graft-versus-host disease prevention in high-risk HCT: lower TNFR1 levels correlate with better outcomes. Biology of blood and marrow transplantation. 2012;18(10):1525-32.

54. Perkey E, Maillard I. New Insights into Graft-Versus-Host Disease and Graft Rejection. Annual Review of Pathology: Mechanisms of Disease. 2018;13:219-45.

55. Wabnitz GH, Michalke F, Stober C, Kirchgessner H, Jahraus B, van den Boomen DJ, et al. L-plastin phosphorylation: A novel target for the immunosuppressive drug dexamethasone in primary human T cells. European journal of immunology. 2011;41(11):3157-69.

56. Latouche A, Allignol A, Beyersmann J, Labopin M, Fine JP. A competing risks analysis should report results on all cause-specific hazards and cumulative incidence functions. Journal of clinical epidemiology. 2013;66(6):648-53.

57. Wolbers M, Koller MT, Stel VS, Schaer B, Jager KJ, Leffondre K, et al. Competing risks analyses: objectives and approaches. European heart journal. 2014;35(42):2936-41.

국문 초록

질량분석기 기반의 단백질체학 방법론을 이용하여 이식편대숙주병의 발병위험 및 무재발사망률 예측을 위한 혈액 단백질 생체표지자의 발굴 및 검증 연구

이식편대숙주병은 혈액 암 환자에게 동종조혈모세포 이식 후 발생하는 주된 합병증이며, 이식 후 발생하는 무재발사망률의 가장 큰 비율을 차지하고 있어 동종조혈모세포 이식을 치료 목적으로 널리 이용하는데 심각한 장벽이었다. 급성이식편대숙주병의 발병을 예측할 수 있는 단일 단백질 혹은 여러 단백질의 조합으로 이루어진 바이오마커 패널에 대한 연구가 있었으나 명확하게 발병위험도를 예측할 수 있는 바이오마커는 없었다.

본 연구는 질량분석기를 기반으로 한 단백질체학 분석 기술을 이용하여 동종 조혈모세포 이식을 받은 환자의 혈액에서 급성이식편대숙주병의 발병과 무재발사망률을 예측할 수 있는 새로운 단백질 표지자를 발굴 및 검증을 목표로 하였다. 악성 혈액 질환으로 서울대학교병원에 내원하여 동종 조혈모세포 이식을 시행 받고 연구 목적의 검체 공여에 동의한 환자들로부터 조혈모세포 이식 후 일주일 간격으로 순차적으로 수집된 혈액 검체를 이용하여 단백질 표지자 후보군 발굴을 위한 단백질체학 연구를 수행하였다. 조혈모세포 이식 후 급성이식편대숙주병이 진단받은 5명의 환자에게서 발병시기와 비슷한

혈액검체를 섞어 하나의 실험군 검체로 만들고 비슷한 기간 동안 발병하지 않은 5명의 환자 검체를 섞어 하나의 대조군을 만들었다. 혈장 단백질들을 전처리하여 펩타이드로 만든 뒤 나노액체크로마토그래피-고분해능 질량분석기를 이용하여 단백질들을 동정하였고 상대적인 정량값을 얻었다. 총 202개의 혈장 단백질을 확인하였고 여기서 최종 10개의 DEPs를 추출하였다. 10개의 단백질에서 선정한 34개의 heavy peptide를 합성한 후 질량분석기 기반의 다중반응감지법을 이용한 질량분석법을 개발하여 발굴연구에서 이용한 10명의 개별 환자의 펩타이드의 상대적인 정량값을 측정하였다. GVHD가 발생한 그룹의 검체에서 통계적으로 유의하게 높게 발현된 7개의 표지자 후보 단백질을 선정 후 이로부터 총 14개의 펩타이드를 선정하여 질량분석기 기반의 다중반응감지법을 이용한 절대정량 분석법을 개발하였다. 총 88개의 최적화된 질량지문의 쌍을 개발하여 89명의 독립적인 환자 cohort에서 7개의 단백질의 절대 정량값을 측정하였다.

이들의 정량값과 환자의 임상적 특성 변수 데이터를 이용하여 급성이식편대숙주병과 무재발사망을 예측할 수 있는 다변량 Cox 비례위험모델 (multivariable cox proportional hazard regression model)을 구축하였다. 각 후보 표지자 단백질의 값이 높은 환자들에서 낮은 환자들에 비해 급성이식편대숙주병과 무재발사망이 높게 나오는 경향을 보였다. 모델구축 후 선정한 3 개의 단백질표지자 후보(TIMP-1, plastin-2, and REG3α) 를 이용하여 0 점부터 3 점까지의 값을 가진 biomarker panel score 변수를 만들었다. Biomarker panel score 를 이용하여 단변수와 다변수 Cox 회귀 모델을 구축하여 평가시 급성이식편대숙주병과 무재발사망률을 매우 유의하게 예측하였다.

Biomarker panel score 와 임상특성변수를 함께 넣고 만든 cox 모델을 우도비율검정법, five-fold cross-validated C (5-CVC) indices, net reclassification improvement (NRI) index 방법으로 평가하였고 환자의 임상특성 변수만 가지고 예측했을 때 보다 두 요소를 가지고 함께 예측하였을 때 급성이식편대숙주병과 무재발사망의 예측능이 향상됨을 확인할 수 있었다.

본 연구는 환자의 혈장에서 질량분석기를 기반으로 하여 발굴, 검증한 단백질 표지자를 조합하여 급성이식편대숙주병 과 무재발사망을 예측에 활용할 수 있는 가능성을 제시하였다. 단백질 표지자 패널을 이용한 위험도를 예측하여 미리 면역억제제 용량을 조절하는 등의 치료를 할 수 있게 되고 위험도가 낮은 환자의 경우 면역억제제의 용량을 미리 감량하여 과다한 면역억제제 투여로 인한 기회 감염의 위험성을 줄이는데 도움을 주게 되어 결과적으로 동종 조혈모세포 이식 성적의 향상과 이식환자의 예후 및 삶의 질을 개선하는데 도움이 될 수 있을 것으로 기대된다.

주요어

이식편대숙주병, 동종조혈모세포이식, 단백질체학, 질량분석기, 다중반응검지법, 표지자 발굴, 표지자 검증

학번: 2014-30909